University of Alabama in Huntsville

Plasma Pulsed Power Generation

Submitted to:
Dr. Robert A. Cassanova
NIAC Director
555A Fourteenth Street NW
Atlanta, GA 30318

Prepared By:

Dr. Clark W. Hawk
Principal Investigator
Tel: (256) 890-7200 Fax: (256) 890-7205
Email: hawkc@email.uah.edu

May 28, 1999

List of Acronyms

BSCCO	$Bi_2Sr_2CaCu_2O_x$
FET	Field-Effect Transistor
HTSC	High Temperature Superconductor
ICF	Inertial Confinement Fusion
MHD	Magnetohydrodynamics
MSFC	Marshall Space Flight Center
NASA	National Aeronautics and Space Administration
NIAC	National Institute for Advanced Concepts
P^3G	Plasma Pulsed Power Generation
PPPG	Plasma Pulsed Power Generation
SMES	Superconducting Magnet Energy Storage
UAH	University of Alabama in Huntsville
YBCO	Yttrium-Barium-Copper-Oxide

Abstract

The objective of this research project was to investigate system level performance and design issues associated with magnetic flux compression devices for spacecraft power generation and propulsion. For the purposes of this research, it is assumed that microfusion detonation technology will become available within a few decades. The ability to ignite pure fusion micro bursts with reasonable levels of input energy is a challenging scientific problem. It remains to be seen whether an effective ignition driver can be developed which meets the requirements for practical spaceflight application (namely high power density, compactness, low weight, and low cost).

The major system development issues include anticipated generator performance, magnetic flux compression processes, magnetic diffusion processes, high temperature superconductor (HTSC) material properties, plasmadynamic processes, detonation plasma expansion processes, magnetohydrodynamic instabilities, magnetic nozzle performance, and thrust production performance. Phase I research validated the proposed concept and defined the major feasibility issues. This included a critical review of the relevant scientific literature, conduct of first-order performance analyses, and conducting small-scale laboratory experiments.

An additional objective of the Phase I research is the definition of a Phase II work plan which addressed the major feasibility issues in a meaningful way and defined a strategy for investigating system performance, development costs, and key enabling technologies as they relate to future space exploration mission architectures. This Phase II work plan was developed within the budget and time constraints of the NIAC program and yet organized such that it produced results that generated continued follow-on interest within NASA.

In the near term, the first demonstration device will utilize high explosive detonation charges in order to establish scientific feasibility since inertial confinement fusion (ICF) technology is still several years away. Indeed, it is believed that practical devices based on high explosive detonations can be developed with existing enabling technologies and demonstrate “proof of principle”.

Executive Summary

The application of pulsed fusion and antimatter reactions as an energy source for propulsion and power devices is gaining increased interest in light of new NASA challenges to explore our solar system and the universe. A key problem to solve is how to extract this energy in meaningful quantities and in a useful manner for such applications. A proposed embodiment (Plasma Pulsed Power Generation or P^3G) has been conceived and was the subject of this study.

The P^3G concept is an advanced systems concept that incorporates the principles of magnetic flux compression for direct conversion of nuclear/chemical detonation energy into electrical power. Specifically, a magnetic field is compressed between an expanding detonation driven diamagnetic plasma and a stator structure formed from a high temperature superconductor (HTSC). The expanding plasma cloud is entirely confined by the compressed magnetic field at the expense of internal kinetic energy. Electrical power is inductively extracted, and the detonation products are collimated and expelled through a magnetic nozzle. The long-term development of this highly integrated generator/propulsion system

opens up revolutionary NASA Mission scenarios for future interplanetary and interstellar spacecraft. The unique features of this concept with respect to future space travel opportunities are as follows:

- ability to implement high energy density chemical detonations or ICF microfusion bursts as the impulsive diamagnetic plasma source;
- high power density system characteristics constrain the size, weight, and cost of the vehicle architecture;
- provides inductive storage pulse power with a very short pulse rise time;
- multimegajoule energy bursts / terawatt power bursts;
- compact pulse power driver for low-impedance dense plasma devices;
- utilization of low cost HTSC material and casting technology to increase magnetic flux conservation and inductive energy storage;
- improvement in chemical/nuclear-to-electric energy conversion efficiency and the ability to generate significant levels of thrust with very high specific impulse;
- potential for developing a small, lightweight, low cost, self-excited integrated propulsion and power system suitable for space stations, planetary bases, and interplanetary and interstellar space travel;
- potential for attaining specific impulses approaching 10^6 seconds, which would enable missions to the outer planets within ten years and missions at interstellar distances within fifty years.

The analyses conducted in support of this program have served to illustrate both the propulsion and power potential of this concept. For example, 5 to 10 gigawatts of power are achievable with fuel consumption rates on the order of 1 gram per second. Specific impulses of 10^6 seconds are achievable with comparable fuel burnup fractions (10-15%) as for the power generation rates cited. The analyses also served to identify the key technical issues associated with making this concept a reality. The use of plasma armatures does introduce substantial technical risks that must be addressed and overcome through research and development. The major uncertainties with the plasma armature approach are summarized as follows:

- ✓ achieving sufficiently high electrical conductivity in the detonation plasma;
- ✓ electron Joule heating effects;
- ✓ field aligned ion flow due to the ambipolar potential
- ✓ assurance of armature rebound;
- ✓ suppression of Rayleigh-Taylor instabilities.

The HTSC stators have associated with them, major uncertainties that may be categorized as follows:

- ✓ breakdown of HTSC under strong applied pulse fields;
- ✓ hysteresis cycling of magnetization;
- ✓ joule/neutron heating of the material;
- ✓ structural integrity under cyclic loading;
- ✓ bulk-processed vs. wire fabrication.

Some experimentation was accomplished to address the feasibility of the HTSC stator. The experiments proved that a BSCCO superconductor provides adequate resistivity to an applied magnetic field. There is a much greater time lag between applied external current and induced magnetic field in a BSCCO superconductor than in regular metals, such as aluminum. The proper magnetic resistivity to an applied field is a key element in proving that type-II high temperature superconductors can be used as stators in a pulsed power generation process. At this point in time no conclusions have been made concerning the magnetic resistivity of a YBCO superconductor; however, this will be an early experiment in Phase II.

1.0 Background and Rationale

NASA has set a number of ambitious mission goals for future space flight. These include such criteria as accomplishing missions to Mars within months rather than years, 10 times improvement in capability within 15 years, 100 times improvement in capability in 25 years and 1000 times improvement in capability in 40 years.[§]

These mission goals have been translated into a power generation goal of 10 kW/kg and a propulsion specific impulse goal of 10,000 seconds.

Power generation is a critical technology for deep space missions.[*] Specifically, solar power no longer can be the primary means for spacecraft power generation, both in terms of the specific power goals and the distances from the Sun where the spacecraft must operate. This presents a technology challenge in devising the means by which power levels of gigawatts might be generated with relatively modest mass consumption.

Propulsion specific impulses of the magnitude cited above are achievable only through a few means for vehicle accelerations appropriate for missions to the planets and near the edges of our solar system. (see Figure 1). Antimatter and pulsed fusion rockets appear to be the most promising for these operating regimes.

Note that both of these energy sources are consistent with a powerplant specific mass of 10 kW/kg. The promise of these energy sources led us to exploring how to devise the means to extract this energy for either or both space power systems and propulsion applications. One such means would incorporate neutron-lean microfusion detonations to form an expanding diamagnetic plasma cloud which compresses the magnetic flux within a semi-enclosed reactor until the plasma expansion is reversed by the increasing magnetic pressure and the detonation products are collimated and expelled through a magnetic nozzle.[1-7]. This approach can capitalize on recent advances in inertial confinement fusion (ICF) technologies including magnetized target concepts and antimatter initiated nuclear detonations.[8-10]. The charged particle expansion velocity in these detonations can be on the order of 10^6-10^7 m/s, and, if effectively collimated by a magnetic nozzle, can yield the Isp and the acceleration levels needed for practical interplanetary flight. Methods for inductively extracting electrical power from the compressed magnetic field can also be envisioned. This latter feature can be used either for spacecraft power generation or as a means to extract energy for ignition of subsequent detonations. This means that the Plasma Pulsed Power Generation (P^3G) concept described in the following section and pulsed fusion rockets appear to be the most promising for these operating regimes.

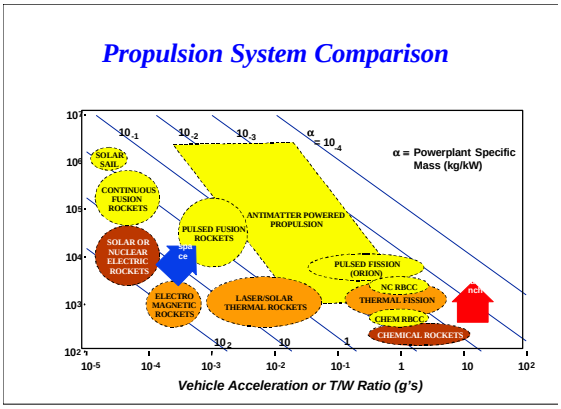

Fig. 1 Advanced Propulsion Performance Regimes

[§] Speech by Arthur Stephenson, Director, NASA Marshall Space Flight Center, April 7, 1999, University of Alabama in Huntsville.

[*] "Space Technology for the New Century", Committee on Advanced Space Technology, Aeronautics and Space Engineering Board, National Research Council, 1998.

2.0 Advanced Concept Description

2.1 System Approach and Attributes

The desire for fast, efficient interplanetary transport requires propulsion systems having short acceleration times and very high specific impulse attributes. Unfortunately, most highly efficient propulsion systems which are within the capabilities of present day technologies are either very heavy or yield very low impulse such that the acceleration time to final velocity is too long to be of lasting interest. One exception, the nuclear thermal thruster, could achieve the desired acceleration but it would require inordinately large mass ratios to reach the range of desired final velocities. A particularly promising alternative approach, among several competing concepts that are beyond our modern technical capabilities, is a pulsed thermonuclear fusion thruster. In this scheme, neutron-lean microfusion detonations form an expanding diamagnetic plasma cloud which compresses the magnetic flux within a semi-enclosed reactor structure until the plasma expansion is reversed by increasing magnetic pressure and the detonation products are collimated and expelled by a magnetic nozzle.[1-7] This approach could capitalize on recent advances in inertial confinement fusion (ICF) technologies including magnetized target concepts and antimatter initiated nuclear detonations.[8-10] The charged particle expansion velocity in these detonations can be on the order of $10^6 - 10^7$ m/s and if effectively collimated by a magnetic nozzle, can yield the Isp and acceleration levels needed for practical interplanetary flight. Methods for inductively extracting electrical power from the compressed magnetic field can also be envisioned. This is an integral component of the scheme since the energy needed to ignite the subsequent detonation is extremely high. Furthermore, an indirect mode of operation is conceivable in which a detonation driven magnetic compression generator is used to power electric thrusters.

The Plasma Pulsed Power Generator (P^3G) is an advanced systems concept that incorporates the principles of magnetic flux compression for direct conversion of nuclear/chemical detonation energy into electrical power. Specifically, a magnetic field is compressed between an expanding detonation driven diamagnetic plasma and a stator structure formed from a high temperature superconductor (HTSC). The expanding plasma cloud is entirely confined by the compressed magnetic field at the expense of internal kinetic energy. Electrical power is inductively extracted, and the detonation products are collimated and expelled through a magnetic nozzle. The long-term development of this highly integrated generator/propulsion system opens up revolutionary NASA Mission scenarios for future interplanetary and interstellar spacecraft. The unique features of this concept with respect to future space travel opportunities are as follows:

- ability to implement high energy density chemical detonations or ICF microfusion bursts as the impulsive diamagnetic plasma source;
- high power density system characteristics constrain the size, weight, and cost of the vehicle architecture;
- provides inductive storage pulse power with a very short pulse rise time;
- multimegajoule energy bursts / terawatt power bursts;
- compact pulse power driver for low-impedance dense plasma devices;
- utilization of low cost HTSC material and casting technology to increase magnetic flux conservation and inductive energy storage;
- improvement in chemical/nuclear-to-electric energy conversion efficiency and the ability to generate significant levels of thrust with very high specific impulse;

- potential for developing a small, lightweight, low cost, self-excited integrated propulsion and power system suitable for spacestations, planetary bases, and interplanetary and interstellar space travel;
- potential for attaining specific impulses approaching 10^6 seconds, which would enable missions to the outer planets within ten years and missions at interstellar distances within fifty years.

2.2 Detailed Technical Description

The plasma pulsed power generator (P^3G) is based on a three step energy conversion process: chemical/nuclear → kinetic → electrical. The initial detonation charge is first transformed into kinetic energy as a rapidly expanding diamagnetic plasma cloud. The kinetic energy of the plasma is then transformed into electrical energy through electromagnetic field interactions.[11] The efficiency of the former conversion process is governed by the detailed physics of the detonation processes and can be estimated with some degree of confidence as a result of intense investigation of ICF concepts over several decades. The efficiency of the latter conversion process is more problematic and heavily dependent on system design. Ideally, the energy conversion efficiency can exceed 50%, but this value could be reduced substantially by real plasma processes such as flute instabilities, electron Joule heating effects, and field aligned ion flow due to the ambipolar potential. Furthermore, the magnetic field configuration and reactor chamber design plays a significant role in terms of magnetic diffusion losses and magnetic flux compression efficiency.

The P^3G system is illustrated for a radial mode configuration in Fig. 2, although other geometrical configurations can be envisioned for the reaction chamber (e.g., spherical). For simplicity, the generator is depicted as a single turn induction coil connected to a single turn load coil. The induction coil serves as a stator while the expanding plasma serves as an armature. The circuit diagram for the generator is shown as a time varying generator inductance (L_g) connected to a fixed load inductance (L_L) with a resistive loss component (R). The principle of operation is as follows:

- seed flux injection;
- ignition of the centrally located explosive charge;
- detonation driven expansion of the plasma armature;
- magnetic flux trapping between the plasma armature and the stator coil with magnetic flux diffusion into both the stator and armature;
- rapid magnetic flux compression as the kinetic energy of the plasma is transformed into magnetic pressure;
- forced reduction in generator inductance yielding a fast rise time current pulse.

The circuit equation for the generator may be written in differential form as

$$\frac{d}{dt}(Li) + Ri = 0 \tag{1}$$

where $L = L_g + L_L$ and i is the instantaneous current. Solving for the current, we obtain

$$i = \frac{L_0 i_0}{L} \exp\left\{-\int_0^t (R/L)dt\right\} \tag{2}$$

and we find that the current varies inversely with the generator inductance. It is convenient to rewrite Eq. (2) in terms of a flux coefficient λ

$$l = \frac{f}{f_0} = \frac{Li}{L_0 i_0} = \exp\left\{-\int_0^t (R/L)dt\right\} < 1 \tag{3}$$

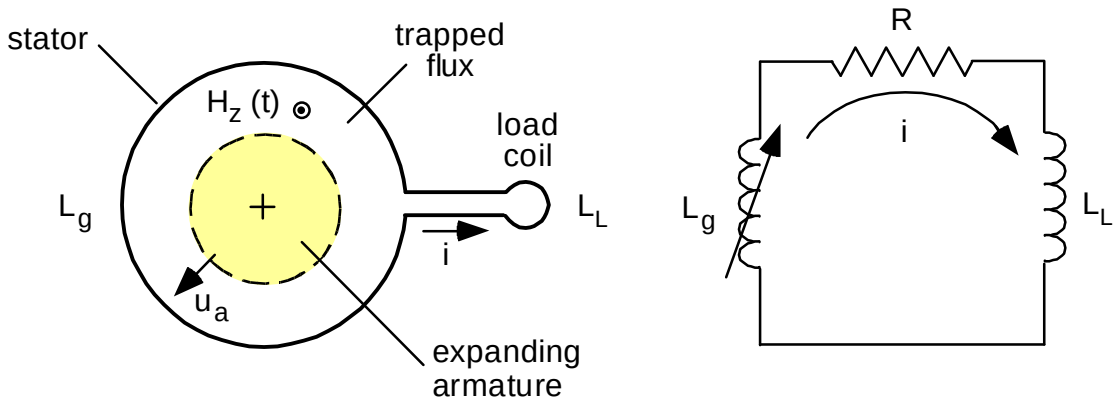

Figure 2: Schematic of radial mode flux compression generator and circuit diagram.

where ϕ is the magnetic flux. Thus, λ is a measure of flux compression efficiency and quantifies the magnetic flux diffusion losses into the stator and the armature through a negative exponential function. The magnetic diffusion processes are illustrated in Fig. 3. It is worth noting that the expression for the flux coefficient demonstrates that flux diffusion losses can be effectively expressed in terms of a resistive circuit component.

The energy delivered to the load inductance W_L is defined by

$$W_L = \frac{1}{2} l i^2 \tag{4}$$

and substitution of Eq. (3) yields

$$W_L = W_0 \left(\frac{L_0}{L} \right) \left(\frac{l}{L} \right) \exp\left\{ -2 \int_0^t (R/L) dt \right\} \tag{5}$$

where $W_0 = \frac{1}{2} L_0 i_0^2$ is the initial inductively stored energy. The power delivered to the load P_L is defined by

$$P_L = v_L i = l \frac{di}{dt} i \tag{6}$$

We note, however, that $W_L = \frac{1}{2} \lambda i^2$ and that Eq. (1) can be written as

$$\frac{di}{dt} = -i \left(R + \dot{L}_g \right) / L \tag{7}$$

Thus, the delivered power takes the form

$$P_L = -2 W_L \left(R + \dot{L}_g \right) / L \tag{8}$$

The major point to emphasize in this simple development is the importance of magnetic diffusion losses to generator performance. For example, the current multiplication ratio varies in direct proportion to λ ($i/i_0 \sim \lambda$), and the energy multiplication ratio varies in direct proportion to λ^2 ($W_L/W_0 \sim \lambda^2$). For good generator performance it is essential to minimize these diffusion losses by achieving low magnetic diffusivity characteristics in both the stator and armature. The fundamental definition of magnetic diffusivity in terms of material properties is

$$D_m = \frac{1}{ms} \tag{9}$$

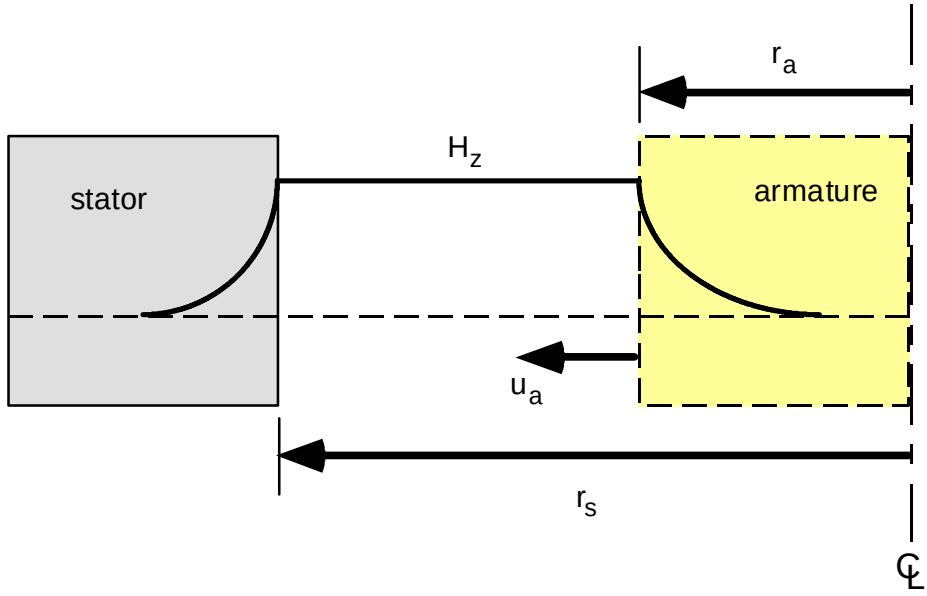

Figure 3: Illustration of magnetic diffusion processes in the stator and armature.

where μ is the magnetic permeability and σ is the electrical conductivity. Thus, it is desirable to utilize materials having the highest possible electrical conductivity.

The P^3G system is an innovative approach to magnetic flux compression in that it envisions the use of a detonation plasma cloud as the armature and the use of a type-II high temperature superconductor (HTSC) as the stator material. When the detonation plasma is formed by a pure fusion micro burst, the hot plasma ball is fully ionized and highly conductive and the magnetic diffusion losses are small. If the detonation plasma is formed by high explosives, however, the electrical conductivity levels achieved are generally marginal although it appears that a practical system could be developed despite the losses. Typically, good performance can be achieved when the stator is fabricated from a highly conductive metal, but the utilization of a type-II HTSC material may offer a method for reducing the magnetic diffusivity, significantly. The end result would be an intermittently fired pulse power driver that could also generate thrust in a proper configuration. This combined propulsion and power capability would open up new space transportation vistas for future NASA missions that are unachievable with current technology.

2.2.1 Armature Issues

The conventional approach in magnetic flux compression generators is to utilize a metal armature to minimize diffusion losses. Usually, the generator coil is surrounded with high explosives and forcibly deformed. In this case, the deformed coil structure serves as an armature. Devices based on this design approach are usually referred to as magnetoimplosive generators and represent a highly mature technology. In principle, it should also be possible to develop a cartridge-loaded radial mode flux compression generator where the cartridge is configured as a detonation charge surrounded by a thin metal liner, as illustrated in Fig. 4 (a). However, the major drawbacks for the explosively driven metal liner approach are (1) the limited detonation speed that can be achieved with high explosives, (2) self-destructive operation which negates the desire for intermittent firing capability, and (3) incompatibility with ICF micro explosion schemes. For example, if one desires high energy output, say 10^7 Joules, large scale devices are required. This implies the need to achieve very fast compression within a large device in order to obtain a fast pulse rise time. Thus, armature speeds are needed which exceed the limit

associated with explosive driven metal liners. The obvious solution is to attempt to utilize a detonation plasma armature as proposed for the P^3G. This concept is illustrated in Fig. 4 (b). By eliminating the metal liner and relying on the electrical conductivity of the plasma to provide the necessary diamagnetic characteristics, it may be possible to obtain the desired compression rate in an intermittently fired device. A comparison of metal vs. plasma armature characteristics is shown in Table I.

The major advantages associated with the use of a plasma armature rather than a metal armature may be summarized as follows:

- ✓ greater speed (shorter pulses);
- ✓ greater expansion;
- ✓ lower cost;
- ✓ lower impulse delivered to generator structure;
- ✓ intermittent firing capability;
- ✓ exhaust products can be utilized for propulsion.

These advantages are of special significance to spaceflight applications where simplicity and robust performance attributes are essential. However, the use of plasma armatures does introduce substantial technical risks that must be addressed and overcome through research and development. The major uncertainties with the plasma armature approach are summarized as follows:

- ✓ achieving sufficiently high electrical conductivity in the detonation plasma;
- ✓ electron Joule heating effects;
- ✓ field aligned ion flow due to the ambipolar potential
- ✓ assurance of armature rebound;

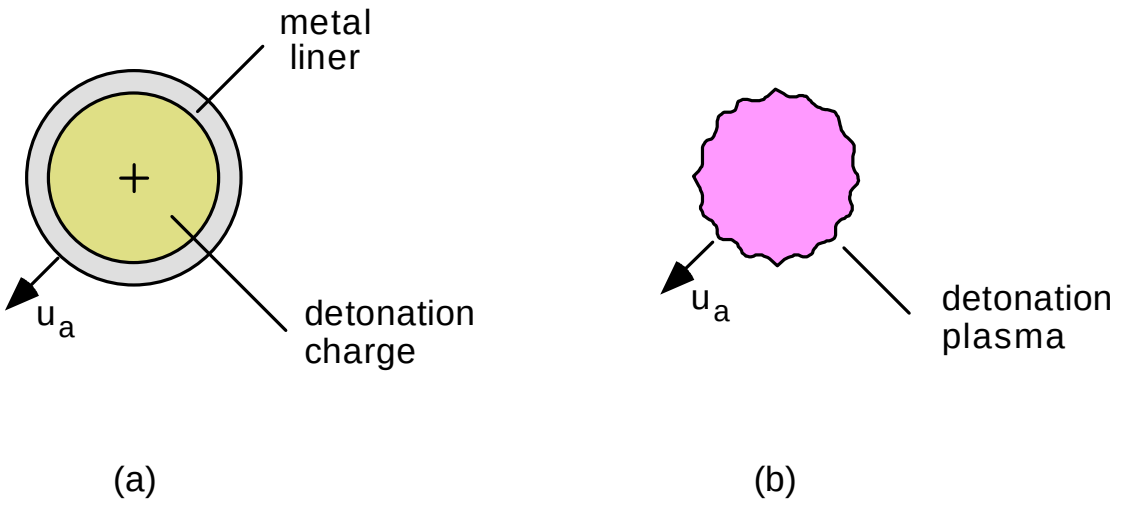

Figure 4: Illustration of an explosively driven metal liner armature based on a metal cased cartridge (a) and a detonation plasma armature (b).

Table I: Metal vs. Plama Armature Characteristics

Parameter	**Metal Armature**	**Plasma Armature**
conductivity	very high	relatively low
temperature	very low	very high
velocity	very low	very high

2.2.2 Stator Issues

A unique and innovative feature of the P^3G concept is the utilization of a type-II HTSC reaction chamber to confine the magnetic field as it is compressed outwardly by the expanding plasma. Although it is possible to utilize highly conductive metals as the stator material, a type-II HTSC stator should be able to substantially reduce magnetic diffusion losses and significantly improve energy conversion efficiency.

Superconductors are divided into two types depending on their characteristic behavior in the presence of a magnetic field. Type-I superconductors comprised of pure metals tend to repel a penetrating magnetic flux due to the Meissner effect. In principle, when a magnetic field line attempts to penetrate the superconductor surface, eddy currents are established in which microscopic current loops develop a magnetic field that counteract the penetrating field. In the Meissner state, the penetrating field is completely repelled from the interior of the superconductor. For type-I superconductors, the material is either perfectly conducting and exists in the Meissner state or it undergoes a phase transformation to the normal state. The major obstacle to using type-I superconductors in a flux compression application is the low threshold values (i.e., temperature, current density, and magnetic field strength) defining critical transition to the normal state. The maximum critical field for a type-I superconductor is about 0.2 Tesla, which is far too low for practical application in flux compression devices.

Ceramic based type-II superconductors, on the other hand, are potentially useful for flux compression applications due to the high critical threshold values which can be obtained. For example, the critical temperature is above liquid nitrogen temperatures over a wide range of current densities, and superconductivity can persist under applied magnetic fields exceeding 100 Tesla. In a type-II superconductor, however, there are two critical field levels. The first critical field ($B_{c,1}$) defines the limiting value for maintaining a true Meissner state and is normally very small. When the applied field exceeds $B_{c,1}$, the material enters the so called mixed state where the field penetrates in quantized amounts of flux. These points of penetration, known as fluxoids, may be envisioned as circulating vortices of current. The second critical field level ($B_{c,2}$) defines the transition to the normal state, and it can be large enough for practical flux compression application. Flux penetration in both the Meissner state and the mixed state is illustrated schematically in Fig. 5 as well as the characteristic variation of the critical fields for a type-II HTSC.

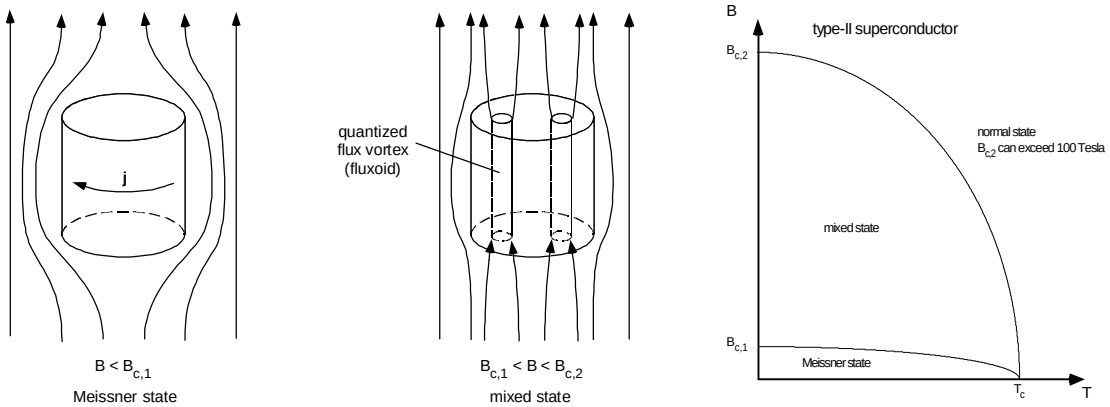

Figure 5: Illustration of superconductor field penetration in the Meissner state and the mixed state and characteristic variation of the critical fields for a type-II HTSC.

The interaction of the fluxoids with defects in the superconductor alters its conductive properties. That is, a fluxoid encompassing or adjacent to a defect has its energy altered and its free motion through the superconductor is inhibited. This phenomenon, known as flux pinning, causes a field gradient in the superconductor and gives rise to a net current in the material. Since the pinning force is small, fluxoids can be broken loose from their pinning centers resulting in a net creep of the flux through the conductor as a function of time. This results in an effective voltage in a type-II superconductor. If the current density is low and the magnetic field is not intense, flux creep is insignificant and the induced voltage and effective resistance will be essentially zero. At very high fields and high current densities, fluxoids will migrate rapidly, giving rise to a phenomenon called flux flow. The effective resistance can be non-negligible in the flux flow case, and breakdown to the normal state can ensue. This can be a particularly exacerbating issue when the flux skin depth is small and the induced current is high, because under these circumstances the current density can be very high and may exceed the critical value for the HTSC.

The important point to emphasize is the fact that the magnetic diffusivity of a type-II superconductor can be several orders of magnitude below that of the best metals, even in flux flow mode. For instance, recent studies investigating the magnetic diffusivity characteristics of various superconductor materials under pulsed magnetic fields indicate that the diffusivity can range from 10^{-2} to 10^{-6} m^2/s.[12,13] This range can be compared with nominal values for various metals as indicated in Table II.

Table II: Electrical and Magnetic Diffusivity Properties of Common Metals

Parameter	Dimension	Copper	Brass	Aluminum	Stainless Steel
ρ_0 (20 °C)	$\mu\Omega\cdot cm$	1.7	6.2	2.8	72
σ_0 (20 °C)	$10^6\ (\Omega\cdot m)^{-1}$	63.3	15.7	39.2	1.38
$D_m=(\mu_0\sigma_0)^{-1}$	m^2/s	1.26	5.10	2.04	58.0

It is clear that for a type-II HTSC, flux penetration will occur under an intense pulsed magnetic field. Therefore, the major questions to be answered are:

(1) How resistant are HTSC materials to magnetic field penetration in the mixed state?
(2) How good are the magnetic diffusion characteristics in the mixed state?
(3) How does the HTSC material behave under intense applied pulse fields? Will it break down?

The hope is that the transient magnetic field diffusion through an HTSC stator in the P^3G system will exhibit a penetration time longer than the characteristic pulse time of the armature expansion process. This concept is illustrated schematically in Fig. 6. Here, we show a section of the HTSC stator wall with an increasing magnetic field H inside the generator. The anticipated magnetic field profiles in the stator wall are shown at various instances in time during the armature expansion process. Note that there is some characteristic time Δt_p defining the penetration time of the magnetic field through the stator and some characteristic time defining the expansion time of the detonation plasma (τ_D). For practical purposes, it is necessary that $\Delta t_p > \tau_D$.

This concept is entirely hypothetical at this point and there are a whole host of significant research issues that must be addressed prior to practical implementation. The major uncertainties may be categorized as follows:

- ✓ breakdown of HTSC under strong applied pulse fields;
- ✓ hysteresis cycling of magnetization;
- ✓ joule/neutron heating of the material;
- ✓ structural integrity under cyclic loading;
- ✓ bulk processed vs. wire fabrication.

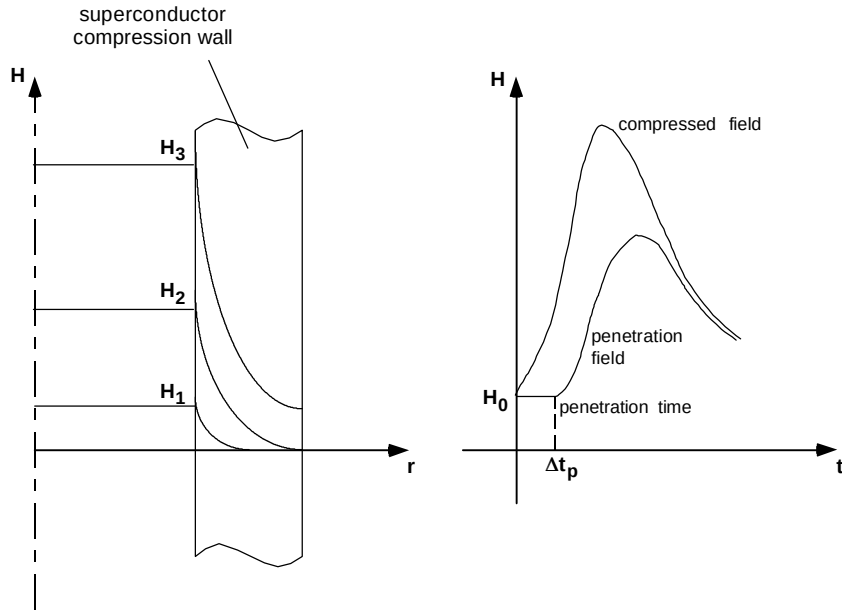

Figure 6: Illustration of transient magnetic field diffusion and penetration through the HTSC stator.

2.2.3 System Configuration

The design configuration of the P^3G system is currently envisioned as a simple radial mode implementation with inductively coupled circuits, as shown in Fig. 7. Fundamentally, the generator consists of three nested concentric shells. The inner most shell is the pick-up (stator) coil in which electrical power is inductively extracted from the flux compression process. It is anticipated that the pick-up coil will be fabricated from HTSC material. The pick-up coil is surrounded by a shielding shell which may or may not be fabricated from a HTSC material in bulk processed form. The purpose of the shielding shell is to minimize induced current transients in the outer superconducting magnet coil whose function is to produce the initial seed flux in the generator. If a nuclear detonation is used as the plasma source, a target pellet would be fired into the reaction chamber and ignited by a high energy driver (i.e., laser beam or particle beam). If a chemical detonation is used as the plasma source, the explosive component could either be fired into the reaction chamber as a target pellet or directly inserted as an expendable cartridge. The P^3G system incorporates the following innovative design features:

- ✓ radially expanding detonation plasma armature;
- ✓ HTSC stator and/or shielding shell (either bulk processed or wire coil);
- ✓ effective reduction in self inductance through an increase in mutual inductance;
- ✓ no deformation of circuit elements;
- ✓ magnetic rebound of armature moderates burst effects;
- ✓ non-self-destructive intermittent firing capability;
- ✓ inductive extraction and storage of electrical power.

In practice, all of the individual circuit elements of the P^3G system will interact inductively. The coupling of these circuits is defined by the mutual inductance between the various elements. The elements of major importance to the generator are:

- excitation magnet circuit;
- pick-up coil circuit;
- moving armature circuit.

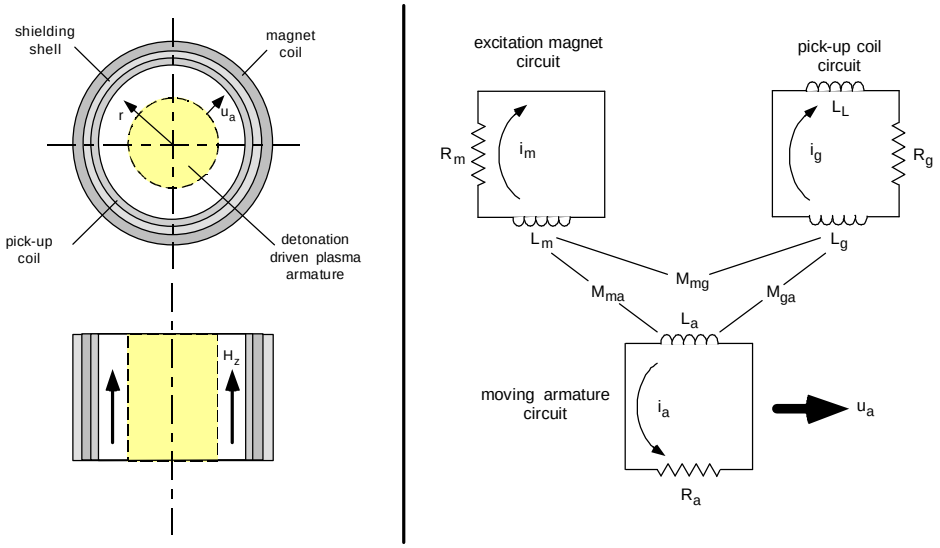

Figure7: Schematic of radial mode PPPG system configuration and inductively coupled circuits.

In a good engineering design, the mutual inductance between the excitation magnetic coil and the other circuit elements in the system will be negligible. For good energy conversion efficiency, the goal is to cause an effective reduction in generator self-inductance through an increase in the mutual inductance between the expanding armature and the pick-up coil. In this way, it is not necessary to deform the circuits.

The envisioned embodiment of the P^3G system incorporates Superconducting Magnet Energy Storage (SMES) technology as a means of inductively storing the extracted electrical power. This approach, illustrated in Fig. 8, is much more compact, lower in weight, and lower in cost than capacitive energy storage technologies. In this system approach, the load coil would be a normal metal conductor while the storage coil would be a superconductor. The SMES coil would be open during pulse generation and immediately closed at peak current. This system would be able to supply the on-demand pulse power needed for ignition of the subsequent nuclear detonation. If the electrical energy is to be used in a normal power grid, several storage coils could be incorporated into the design such that continuous DC power can be conditioned and bussed throughout the spacecraft. An operating P^3G can be expected to supply their own operational power requirements, but it may prove more practical to utilize a chemical explosive driven P^3G as a pulse power source for a pure fusion detonation system.

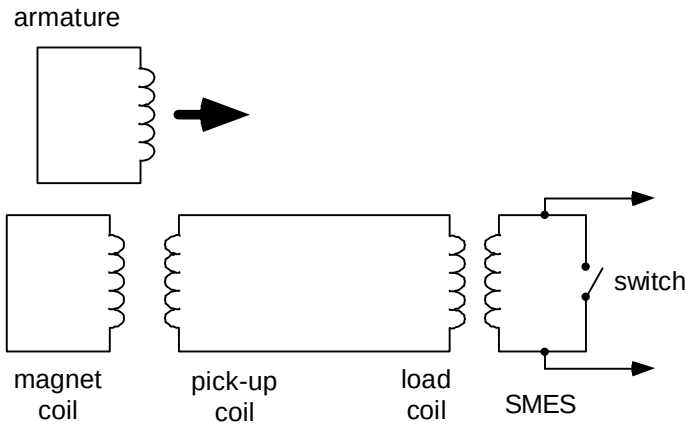

Figure 8: Superconducting magnet energy storage (SMES) circuit coupled to PPPG system.

2.2.4 Space Propulsion Applications

The principle of magnetic flux compression also has important implications with respect to direct thrust production using nuclear detonations. In the seminal Orion class nuclear pulse rocket concept, momentum from a nuclear detonation is directly absorbed by a massive pusher plate attached to the vehicle.[14,15] But it is also possible to control and direct the detonation plasma with electromagnetic fields when using a neutron-lean fusion detonation pulse. This concept, first introduced by Winterberg, is based on the use of a concave magnetic mirror to redirect the particle fluxes.[1] Along these lines of thought, it would appear advantageous and feasible to consider an approach which combines the electrical power production function and the thrust production function within a single highly integrated system. One possible implementation of this approach is the Winterberg/Daedalus class magnetic compression reaction chamber shown in Fig. 9. By incorporating the essential ideas of the P^3G concept, it is possible to reduce flux diffusion losses, reduce the minimum seed field, and reduce the overall size of the reaction chamber. The result is a compact, low weight integrated propulsion and power system driven by low yield nuclear fusion detonation pulses that can yield acceptable interplanetary trip times while carrying sufficient payload to perform meaningful missions.

In this concept, the fusion plasma expands against a rearward diverging magnetic field provided by a set of superconducting coils. The magnetic flux is trapped and compressed between the plasma and a conductive reaction chamber wall (i.e., HTSC stator). The increased magnetic pressure acting on the plasma forces it out the rear of the reaction chamber. The compressed magnetic field also produces a magnetic pressure on the reaction chamber wall yielding a forward thrust component. Electrical power is extracted from the flux compression process using an inductive pick-up coil located at the exit of the reaction chamber. This concept depends on the use of fusion fuels having a low neutron yield such as D-He^3.

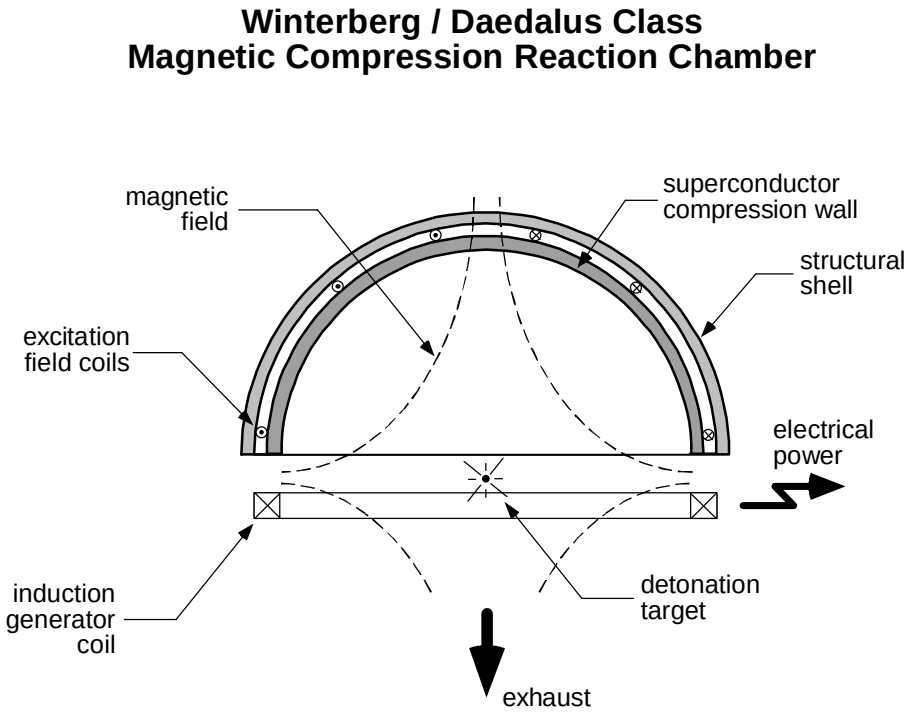

Figure 9: Winterberg/Daedalus class magnetic compression reaction chamber for integrated space propulsion and power applications.

A nuclear pulse system based on this scheme can provide performance levels in the required regime of both high jet power and high Isp. Along these lines, it is instructive to compute the theoretical performance limits that can be achieved for various fusion fuels. We begin with the assumption that after the nuclear reactions are quenched by the hydrodynamic disassembly, the fusion energy is averaged by collisions among all the particles in the plasma including the blowoff mass which did not undergo reaction. After complete thermalization, the energy per ion is the same throughout the fireball and we can write the following relationship for energy conservation:

$$\frac{1}{2} m_i u_i^2 = \frac{f_b \Delta m c^2}{N_i} \tag{10}$$

where m_i is the mass of ion i, u_i is the velocity of ion i, f_b is the burn fraction, Δm is the total mass defect for the fusion reaction, c is the speed of light, and N_i is the number of ion species. Because the neutrons are isotropically distributed, they are ineffective for direct thrust production purposes. Only the momentum of charge particles can be manipulated for direct thrust production. By introducing a parameter for the mass fraction that is converted to energy by the reaction ($\alpha = \Delta m/m_R$), it is possible to write Eq. (10) in the form:

$$\frac{1}{2} m_i u_i^2 = \frac{f_b \alpha m_R c^2}{N_i} \tag{11}$$

where $m_R = \Sigma_R m_i$. From momentum conservation considerations, we obtain the following relationship:

$$\overline{m}_i \overline{u}_i = \frac{1}{2}\left[(1 - f_b)\sum\nolimits_R m_i u_i + f_b \sum\nolimits_P m_i u_i\right] \tag{12}$$

where the overbar denotes an average over all ion species. We can now use Eq. (11) to eliminate u_i on the right hand side of Eq. (12) such that we obtain an expression for the effective ion expansion velocity as a function of the burn fraction.

$$\overline{u}_i = \left[(1 - f_b)\sum\nolimits_R \sqrt{m_i} + f_b \sum\nolimits_P \sqrt{m_i}\right] \frac{1}{\sqrt{2}\overline{m}_i} \sqrt{\frac{f_b \alpha m_R c^2}{N_i}} \tag{13}$$

where the mean ion mass is defined by

$$\overline{m}_i = \frac{1}{2}\left[(1 - f_b)\sum\nolimits_R m_i + f_b \sum\nolimits_P m_i\right] \tag{14}$$

The theoretical Isp may now be computed by noting that

$$Isp = \frac{I}{m} = \frac{m\overline{u}_i}{m} = \overline{u}_i \tag{15}$$

or, when referenced to the earth's gravitational field,

$$Isp = \frac{\overline{u}_i}{g_0} \tag{16}$$

where $g_0 = 9.81$ m/s^2.

The nuclear fusion reactions of practical interest involve isotopes of hydrogen such as deuterium (D) and tritium (T) and isotopes of helium. These reactions are given in Table III where the subscripts denote the nuclear charge (i.e., number of protons) and the superscripts denote the atomic mass number (i.e., total number of nucleons). The proton and neutron branches of the D-D reaction have similar valued cross sections such that each branch consumes roughly 50% of the fuel. The energy yield parameters for the various fusion reactions are given in Table IV. It is important to note that the D-T and D-D reactions have lower fusion cross-sections than the D-He reaction and are easier to ignite; however, they release

about 80% and 35% of the reaction energy in the form of neutrons which are useless for flux compression and wasteful for space propulsion applications since they cannot be manipulated by electromagnetic means. Practical considerations compel the use of D-He as a fusion fuel for space power and propulsion. Although the required ignition energy is substantially higher for D-He, the reaction products will consist predominately of charged particles, which can be electromagnetically manipulated. Of course, there will always be some neutron production due to D-D reactions of the primary fuel and D-T reactions between the primary deuterium and secondary tritium. However, calculations indicate that the number of neutron reactions can be less than 5% of the D-He reactions.

Using the parameters summarized in the tables above, it is possible to compute the effective detonation expansion velocity and theoretical specific impulse for the D-He fusion reaction of interest using Eqs. (13) and (16). The results of these calculations are shown in Fig. 10 as a function of the burn fraction. Detailed ICF calculations indicate that it should be possible to achieve a burn fraction of at least 10% yielding an effective expansion velocity approaching 10^7 m/s. The Isp in this range will be on the order of 10^6 sec. Note that these calculations represent only a theoretical upper limit.

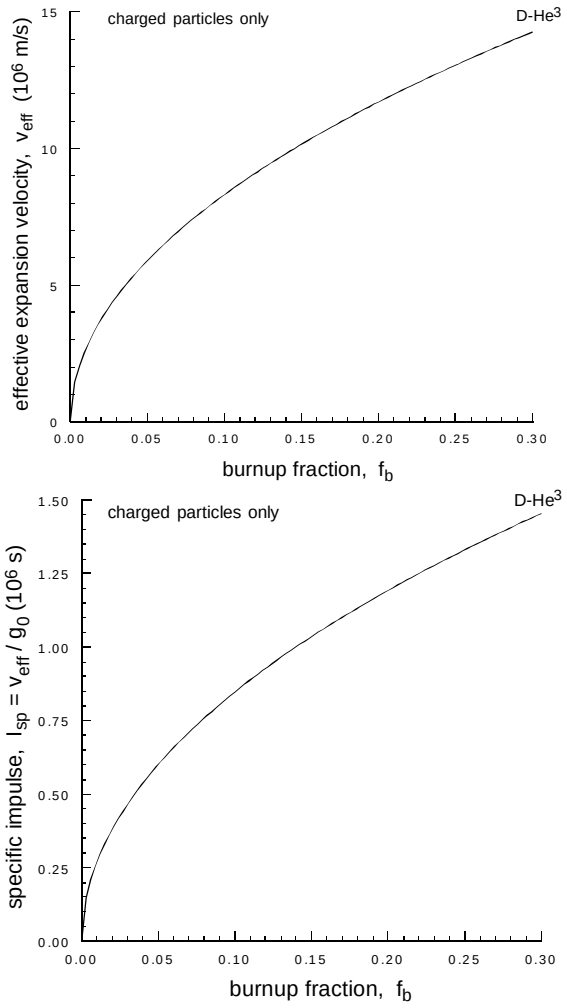

Figure 10: Computed effective expansion velocity and Isp for a D-He fusion detonation.

Table III: Nuclear Fusion Reactions of Major Practical Interest

D-D:	${}_1D^2 + {}_1D^2 \rightarrow {}_1T^3(1.01\ MeV) + {}_1p^1(3.02\ MeV)$	[W = 4.03 MeV]
	$\rightarrow {}_2He^3(0.82\ MeV) + {}_0n^1(2.45\ MeV)$	[W = 3.27 MeV]
D-T:	${}_1D^2 + {}_1T^3 \rightarrow {}_2He^4(3.5\ MeV) + {}_0n^1(14.1\ MeV)$	[W = 17.6 MeV]
D-He:	${}_1D^2 + {}_1He^3 \rightarrow {}_2He^4(3.6\ MeV) + {}_1p^1(14.7\ MeV)$	[W = 18.3 MeV]

Table IV: Energy Yield for Major Fusion Fuels

Fuel	Reaction Products	w (J/kg)	α
D-D	${}_1T^3, {}_1p^1$	9.9×10^{13}	1.1×10^{-3}
D-D	${}_2He^3, {}_0n^1$	8.1×10^{13}	9.0×10^{-4}
D-T	${}_2He^4, {}_0n^1$	3.38×10^{14}	3.75×10^{-3}
D-He	${}_2He^4, {}_1p^1$	3.52×10^{14}	3.91×10^{-3}

The average thrust (T) produced by a nuclear pulse engine is governed by the pulse rate (f_p), the pellet mass (m_p), the magnetic nozzle efficiency (η_j), and the effective expansion velocity as defined by the following relationship:

$$T = h_j f_p m_p \bar{u}_i \qquad (17)$$

The average thrust of an engine using 200 MJ yield fusion detonations of D-He at a pulse rate of 100 Hz is shown as a function of burn fraction in Fig. 11. This calculation assumes a 65% nozzle efficiency. When assuming a constant energy yield, the average thrust decreases with increasing burn fraction since the pellet mass is decreasing with increasing burn efficiency.

By the same token, the Isp will increase with increasing burn efficiency. At a burn fraction of 10%, the average thrust is about 3 kN for the assumed conditions.

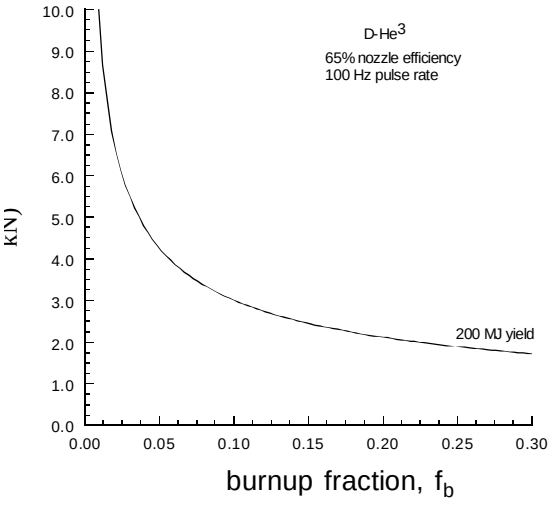

Figure 11 Average engine thrust vs. burnup fraction

3.0 Research Objectives

The objective of this research project is to investigate system level performance and design issues associated with magnetic flux compression devices for spacecraft power generation and propulsion. It is not aimed at the development of technology for producing a microfusion detonation. Pure fusion detonation technology is under active and intense study by various national labs for future energy production applications. For the purposes of our study, it is assumed that this technology will become available within a few decades. The ability to ignite pure fusion micro bursts with reasonable levels of input energy is a challenging scientific problem. It remains to be seen whether an effective ignition driver can be developed which meets the requirements for practical spaceflight application (namely high power density, compactness, low weight, and low cost).

The major system development issues include anticipated generator performance, magnetic flux compression processes, magnetic diffusion processes, HTSC material properties, plasmadynamic processes, detonation plasma expansion processes, magnetohydrodynamic instabilities, magnetic nozzle performance, thrust production performance, and the development of relevant cost/benefit metrics. Phase I research was directed at validation of the proposed concept and definition of the major feasibility issues. This included a critical review of the relevant scientific literature, conduct of first-order performance analyses, and conduct of small-scale laboratory experiments.

An additional objective of the Phase I research was the definition of a Phase II work plan which addressed the major feasibility issues in a meaningful way and outlined a strategy for investigating system performance, development costs, and key enabling technologies as they relate to future space exploration mission architectures. This Phase II work plan had to be developed within the budget and time constraints of the NIAC program and yet organized such that it produced results that were likely to generate continued follow-on interest from NASA.

4.0 Phase I Research

4.1 Performance Modeling

The P^3G system is a cylindrical flux compression generator in which an initial axial magnetic field is compressed between an expanding detonation plasma and a superconducting stator. A simplified schematic of the device was presented in Fig. 2 along with a circuit diagram. In addition, an analysis of the circuit equation was carried out in the previous section demonstrating the importance of the flux compression coefficient λ (a measure of flux diffusion losses) to generator performance. The critical performance impact of flux diffusion losses into the plasma armature and the stator was thoroughly discussed. Indeed, it was the concern over flux diffusion losses that led to the suggestion of HTSC materials for stator applications, and flux diffusion into the plasma armature represent a major feasibility issue for this concept. In Phase I an effort was made to develop a simple first-order analysis methodology to assess anticipated generator performance. This analysis attempted to quantify flux diffusion losses and armature rebound criteria. Before presenting this analysis, however, it is instructive to examine the governing magnetohydrodynamic and electromagnetic equations.

4.1.1 Governing MHD/Electromagnetic Equations

The conservation equations for MHD flow including magnetic fields, Lorentz forces, and Ohmic heating are presented in vector form as follows:

$$\frac{Dr}{Dt} = -r\nabla\cdot\mathbf{u} \tag{18}$$

$$r\,\frac{D\mathbf{u}}{Dt} = -\nabla p + \mathbf{F}_m \tag{19}$$

$$r\,\frac{De}{Dt} = \frac{p}{r}\frac{Dr}{Dt} + \frac{j^2}{s} + \nabla\cdot(k\nabla T) \tag{20}$$

where $\mathbf{F}_m = \mathbf{j}\times\mathbf{B}$ is the magnetic body force and $D/Dt = \partial/\partial t + \mathbf{u}\nabla$ is the substantial derivative. The system also requires an equation of state $p = p(t,\rho)$ and a knowledge of the internal energy properties of the media $e = e(T,\rho)$.

Maxwell's equations govern the electromagnetic processes in the flow field and may be written in vector form as:

$$\nabla\times\mathbf{H} = \mathbf{j} \tag{21}$$

$$\nabla\times\mathbf{E} = -\frac{\partial\mathbf{B}}{\partial t} \tag{22}$$

$$\nabla\cdot\mathbf{B} = 0 \tag{23}$$

$$\nabla\cdot\mathbf{D} = r_e \tag{24}$$

where the following isotropic medium relationships are assumed:

$$\mathbf{B} = m\mathbf{H}; \quad m = m_0 m_R \tag{25}$$

$$\mathbf{D} = m\mathbf{E}; \quad e = e_0 e_R \tag{26}$$

In a medium moving with velocity **u**, the electric field detected by an observer moving with the medium is given by

$$\mathbf{E}^* = \mathbf{E} + \mathbf{u} \times \mathbf{B} \tag{27}$$

and a generalized Ohm's law may be written in the form:

$$\mathbf{j} = s\left[\mathbf{E} + \mathbf{u} \times \mathbf{B}\right] = s\mathbf{E}^* \tag{28}$$

Upon substituting Eq. (28) into Ampere's law as given by Eq. (22), we obtain the following relationship:

$$\nabla \times \mathbf{E}^* = -\frac{D}{Dt}(m\mathbf{H}) - m\mathbf{H}(\nabla \cdot \mathbf{u}) + (m\mathbf{H} \cdot \nabla)\mathbf{u} \tag{29}$$

We now consider the special case of cylindrical one-dimensional geometry (radius and time as independent variables) with a purely axial magnetic field (H_z, E_θ^*, j_θ, u_r). In this case, the MHD equations may be written in the following component form:

$$\frac{Dr}{Dt} = -\frac{r}{r}\frac{\partial}{\partial r}(ru_r) \tag{30}$$

$$r\,\frac{Du_r}{Dt} = -\frac{\partial p}{\partial r} + j_q\, mH_z \tag{31}$$

$$r\,\frac{De}{Dt} = -\frac{r}{r}\frac{\partial r u_r}{\partial t} + \frac{j_q^2}{s} + \frac{1}{r}\frac{\partial}{\partial r}\left(kr\frac{\partial T}{\partial r}\right) \tag{32}$$

where $D/Dt = \partial/\partial t + u_r\,\partial/\partial r$. Faraday's law and Ampere's law, given by Eqs. (21) and (22), respectively, become

$$\frac{\partial H_z}{\partial r} = -j_q \tag{33}$$

$$\frac{1}{r}\frac{\partial}{\partial r}\left(rE_q^*\right) = -m\frac{DH_z}{Dt} - m\frac{H_z}{r}\frac{\partial}{\partial r}(ru_r) \tag{34}$$

and the generalized Ohm's law becomes

$$j_q = sE_q^* \tag{35}$$

where

$$E_q^* = E_q - mH_z u_r \tag{36}$$

By eliminating j_θ and E_θ* in Eqs. (33) through (36), we obtain a generalized diffusion equation for the magnetic field.

$$\frac{DH_z}{Dt} = -\frac{1}{mr}\frac{\partial}{\partial r}\left(\frac{r}{s}\frac{\partial H_z}{\partial r}\right) + \frac{H_z}{r}\frac{Dr}{Dt} \tag{37}$$

Using the continuity relationship of Eq. (30) to eliminate $D\rho/Dt$ gives

$$\frac{DH_z}{Dt} = \frac{1}{mr}\frac{\partial}{\partial r}\left(\frac{r}{s}\frac{\partial H_z}{\partial r}\right) - \frac{H_z}{r}\frac{\partial}{\partial r}(ru_r) \tag{38}$$

Equations (30), (31), (32), and (38) constitute the governing differential relationships for the generator and are to be solved with an appropriate equation of state and constituent laws.

Formal solution of this system of equations requires the implementation of a numerical code which is beyond the scope of the Phase I project. Applicable MHD codes have already been developed, however, at various National Labs and could be adapted for this problem in a Phase II program. Indeed, as part of the Phase I effort, we have researched the literature and identified a Lagrangian MHD algorithm developed at the Sandia National Laboratory that could be implemented with minimal effort.[16] For Phase I purposes, however, a simplified analysis procedure suffices for feasibility assessment purposes.

4.1.2 Magnetic Reynolds Number

Dimensional analysis of the governing MHD equations yields several nondimensional parameters of major importance to MHD flows. One of the more crucial parameters is the magnetic Reynolds number which may be defined as:

$$R_m = \frac{B_{ind}}{B_{app}} = m_0 s_0 u_0 L_0 \tag{39}$$

where the 0 subscript denotes an appropriate characteristic value for the problem. In a general sense, R_m may be thought of as a relative measure of the induced magnetic field in the plasma (B_{ind}) with respect to the external applied magnetic field (B_{app}). Because the magnetic Reynolds number is inversely related to the magnetic diffusivity D_m

$$R_m = \frac{u_0 L_0}{D_m} \tag{40}$$

it is clear that for magnetic Reynolds numbers greater than unity, where the induced field is at least as strong as the applied field, the plasma will be resistive to magnetic diffusion. That is, the induced field associated with eddy currents in the plasma act in an opposing direction to the applied field, and if the induced field is high enough, the plasma interface effectively behaves as a magnetic compression surface.

The important point to note here is that the magnetic Reynolds number depends primarily on the product σu such that one would desire high electrical conductivity and high expansion velocities in order to achieve low flux diffusion losses. For fusion detonations, both of these parameters are extremely high and $R_m >> 1$, as desired. For chemical detonations, the characteristic values are marginal and $R_m > 1$ can be achieved using carefully designed plasma jet sources.

4.1.3 Field Amplification

During the explosive expansion of the plasma armature, we know that some fraction of the trapped magnetic flux will diffuse into the armature and the stator. The flux which escapes from the annular containment region is lost for further compression and represents an inefficiency in generator performance. The field amplification, including losses, may be expressed in terms of the flux coefficient as defined by Eq. (3).

$$l = \frac{f}{f_0} = \frac{B\left(pr_s^2 - pr_a^2\right)}{B_0\left(pr_s^2 - pr_i^2\right)} = \frac{H\left(pr_s^2 - pr_a^2\right)}{H_0\left(pr_s^2 - pr_i^2\right)} \tag{41}$$

or

$$\frac{H}{H_0} = l\,\frac{\left(r_s^2 - r_i^2\right)}{\left(r_s^2 - r_a^2\right)} \tag{42}$$

where r_s is the internal radius of the magnetic flux containment stator, $r_I << r_s$ is the initial radius of the armature, and $r_a(t)$ is the time dependent radius of the plasma armature.

Differentiation of Eq. (42) yields

$$\frac{1}{H_0}\frac{dH}{dt} = 2\,l\,u_a\,\frac{r_a\left(r_s^2 - r_i^2\right)}{\left(r_s^2 - r_a^2\right)^2} + \left(\frac{r_s^2 - r_i^2}{r_s^2 - r_a^2}\right)\frac{dl}{dt} \tag{43}$$

where $u_a = dr_a / dt$. Using Eq. (42) we obtain

$$\frac{1}{H_0}\frac{dH}{dt} = 2\,l\,u_a\,\frac{H}{H_0}\frac{1}{l}\frac{r_a}{\left(r_s^2 - r_a^2\right)} + \frac{H}{H_0}\frac{1}{l}\left|\frac{dl}{dt}\right| \tag{44}$$

or

$$\frac{1}{H_0}\frac{dH}{dt} = \frac{2r_a}{r_s^2 - r_a^2}\,u_a - \frac{1}{l}\left|\frac{dl}{dt}\right| \tag{45}$$

This result demonstrates that the maximum field amplification can occur during armature expansion and not necessarily when $u_a \rightarrow 0$.

An alternative form for field amplification can be developed through the introduction of the flux skin depth, which defines the flux penetration depth during the compression process. The concept of flux skin depth is illustrated in Fig. 12. The flux skin depth is defined by taking the magnetic field at the surface as an effective constant value and requiring that the flux contained within a skin depth s_ϕ be equivalent to the total diffused flux. Because the total flux (contained and leakage) must be conserved, we have

$$mH_0p\left(r_s^2 - r_i^2\right) = mHp\left[\left(r_s + s_{f,s}\right)^2 - \left(r_a - s_{f,a}\right)^2\right] \tag{46}$$

yielding

$$\frac{H}{H_0} = \frac{\left(r_s^2 - r_i^2\right)}{\left(r_s + s_{f,s}\right)^2 - \left(r_a + s_{f,a}\right)^2} \tag{47}$$

Combining Eqs. (42) and (47) gives an expression for λ in terms of the flux skin depths in both the armature and stator.

$$l = \frac{f}{f_0} = \frac{\left(r_s^2 - r_a^2\right)}{\left(r_s - s_{f,s}\right)^2 - \left(r_a - s_{f,a}\right)^2} \tag{48}$$

For a reasonable estimation of the compression dynamics, it is generally sufficient to use appropriate approximations or analytical solutions for s_ϕ. This approach is known as the skin-layer method in which it is assumed that the flux loss and penetration velocity of the diffused magnetic field remain limited. That is, $s_\phi << (r_s - r_a)$, $ds_\phi/dt << u_a$, $s_{\phi,a} << r_a$, and $s_{\phi,s} << d$ where d is the thickness of the stator.

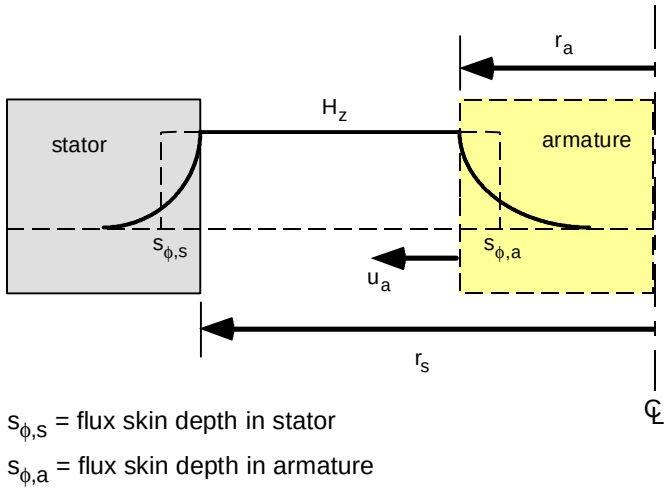

Figure 12: Illustration of flux skin depth concept as applied to the P3G system.

4.1.4 Flux Skin Depth Formulation

In this sub-section, we formulate approximate expressions for the flux skin depth based on analysis of magnetic field penetration into the expanding plasma armature and into the outer superconducting stator.

4.1.4.1 Plasma Armature

To determine the time varying flux skin depth in the expanding plasma armature, we solve the magnetic diffusion equation assuming an exponentially increasing magnetic field $H/H_0 = \chi(t) = e^{t/t_c}$ where τ_c is the characteristic time for magnetic compression and is associated with the plasma expansion speed. The generalized magnetic diffusion equation for a cylindrical one-dimensional geometry (radius and time as independent variables) for a purely axial magnetic field was previously found in the form of Eq. (38).

$$\frac{\partial H_z}{\partial t} + u_r \frac{\partial H_z}{\partial r} + \frac{H_z}{r}\frac{\partial}{\partial r}(r u_r) = \frac{1}{sm}\frac{1}{r}\frac{\partial}{\partial r}\left(r\frac{\partial H_z}{\partial r}\right) \tag{49}$$

In terms of the magnetic induction we obtain the form:

$$\frac{\partial B}{\partial t} + u_r \frac{\partial B}{\partial r} + \frac{B}{r}\frac{\partial}{\partial r}(r u_r) = \frac{1}{sm}\frac{1}{r}\frac{\partial}{\partial r}\left(r\frac{\partial B}{\partial r}\right) \tag{50}$$

where the following initial and boundary conditions apply:

$$u_r(r,0) = u_a(0) \tag{51}$$

$$B(r,0) = 0 \tag{52}$$

$$u_r(r_a,t) = u_a(t) = dr_a/dt \tag{53}$$

$$B(r_a,t) = B_0\, c(t)\ ;\ \ c(t) = e^{t/t_c} \tag{54}$$

$$\left.\frac{\partial B}{\partial r}\right|_{r=0} = 0 \tag{55}$$

This problem involves a moving boundary condition and must be transformed to a space with a stationary boundary. Furthermore, the radial velocity profile inside the plasma armature is required. For the level of approximation of the present analysis, we shall assume that the velocity profile inside the plasma column follows the well known similarity form:[17,18]

$$u_r = \frac{r}{r_a}\frac{dr_a}{dt} \tag{56}$$

This postulate has been applied in many cases involving a column of plasma in a longitudinal magnetic field. At r = 0 and r = r_a, this profile gives exact values for u_r. In the region 0 < r < r_a, this profile provides at least a good estimate of the order of magnitude.

The following transformation variables are now introduced:

$$(r,t) \rightarrow (h,t) \tag{57}$$

where

$$h = \frac{r}{r_a} \tag{58}$$

$$t = \int_0^t \frac{dt}{\sigma\mu r_a^2} \tag{59}$$

Thus,

$$\frac{\partial}{\partial r} = \frac{\partial h}{\partial r}\frac{\partial}{\partial h}\ ;\ \text{where}\ \frac{\partial h}{\partial r} = \frac{1}{r_a} \tag{60}$$

$$\frac{\partial}{\partial t} = \frac{\partial t}{\partial t}\frac{\partial}{\partial t}\ ;\ \text{where}\ \frac{\partial t}{\partial t} = \frac{1}{\sigma\mu r_a^2} \tag{61}$$

Transformation of the diffusion equation from (r,t) space to (η,τ) space yields the following result.

$$\frac{\partial B'}{\partial t} = \frac{1}{h}\frac{\partial}{\partial h}\left(h\frac{\partial B'}{\partial h}\right) \tag{62}$$

where B′ = B$\psi(\tau)$ is the new dependent variable and $\psi(\tau) = r_a^2(t)$. The boundary conditions transform as follows:

$$B'(h,0) = 0 \tag{63}$$

$$B'(1,t) = B_0\, c(t)\psi(t) \tag{64}$$

$$\left.\frac{\partial B'}{\partial h}\right|_{h=0} = 0 \tag{65}$$

The solution to this problem is well known from mathematical physics. The result is

$$B'(h,t) = -B_0 \sum_{n=1}^{\infty} \frac{2b_n J_0(hb_n)}{J_1(b_n)} e^{-b_n^2 t} \int_0^t e^{b_n^2 x}\, c(x)\, y(x)\, dx \tag{66}$$

where β_n are the roots of $J_0(\beta) = 0$. The flux skin depth is now defined such that the diffused flux into the plasma armature $\phi_a(\tau)$ can be expressed by the surface flux density $B(r_a,\tau)$ spread over an annular region of width $s_{\phi,a}$:

$$f_a(t) = B(r_a,t)\left[\pi r_a^2 - \pi\left(r_a - s_{f,a}\right)^2\right] = \int_0^{r_a} B(r,t)\, 2\pi r\, dr \tag{67}$$

It is simple in principle to evaluate Eq. (67) using the solution obtained for the diffused flux profile as expressed by Eq. (66). This yields the following form for the armature flux skin depth:

$$s_{f,a} = r_a\left[1 - \sqrt{1 - 2F(t)}\right] \tag{68}$$

where $F(\tau)$ is a lengthy infinite series involving Bessel functions.

4.1.4.2 Cylindrical Stator

To determine the time varying flux skin depth in the stator, we again solve the magnetic diffusion equation assuming an exponentially increasing magnetic field $H/H_0 = \chi(t) = e^{t/t_c}$ where τ_c is the characteristic time for magnetic compression and is associated with the plasma expansion velocity. Because the exact solution for a hollow cylindrical conductor is very clumsy, we take advantage of a simplifying approximation. That is, when the flux skin depth is much smaller than the radius of the stator cylinder, the diffusion process may be accurately represented by the solution for a planar geometry.

The magnetic diffusion equation for a semi-infinite planar one-dimensional (distance and time as independent variables) geometry with a magnetic field oriented perpendicular to the surface has the form:

$$\frac{1}{D_m}\frac{\partial H}{\partial t} + \frac{\partial^2 H}{\partial V^2} = 0 \tag{69}$$

where the following stationary boundary condition applies

$$H(0,t) = H_0 e^{t/t_c} \quad ; \quad -\infty < t < \infty \tag{70}$$

By seeking a solution of the form $e^{t/t_c}\, f(x)$, we obtain a differential equation for f as

$$\frac{\partial^2 f}{\partial V^2} = \frac{f}{D_{m,s} t_c} \tag{71}$$

from which we deduce the general solution

$$H(V,t) = H_0 e^{t/t_c}\left(A_1 e^{-V/V_0} + A_2 e^{V/V_0}\right) \tag{72}$$

where

$$V_0 = \sqrt{D_{m,s} t_c} \tag{73}$$

The only physically acceptable solution, which satisfies the requirement for a monotonically decreasing field in the conductor, is

$$H(V,t) = H_0 \exp\left(\frac{t}{t_c} - \frac{V}{V_0}\right) \tag{74}$$

Again, the flux skin depth is defined such that the diffused flux $\phi_s(t)$ into the stator can be expressed by the surface flux density $B(r_s,t)$ spread over a depth $s_{\phi,s}$:

$$f_s(t) = B(r_s,t)s_{f,s} = \int_0^\infty B(V,t)dV \tag{75}$$

or

$$H(r_s,t)s_{f,s} = \int_0^\infty H(V,t)dV \tag{76}$$

Thus, evaluation of the integral yields the desired expression for the flux skin depth in the stator.

$$s_{f,s} = V_0 = \sqrt{D_{m,s}t_c} \tag{77}$$

4.1.5 Skin Layer Methodology

A simple estimation of field amplification may be obtained from the "skin layer methodology" if we assume that the surface field increases exponentially during compression.

$$H = H_0 e^{t/t_c} \tag{78}$$

In this case, the following differential relationship must hold true:

$$\frac{dH}{H} = \frac{dt}{t_c} \tag{79}$$

and the characteristic compression time must obey the relation

$$t_c = \frac{H}{dH/dt} \tag{80}$$

Following the methodology of Sakharov, the field rise is arbitrarily considered as a time sequence of exponential functions with variable τ_c governed by Eq. (80).[19] The physical motivation for the skin layer methodology is based on the fact that the skin layer depth is dominated by the ever increasing field so that the contribution from the previous initial condition is rapidly lost. The previously developed approximations for the flux skin depth in the armature and stator assumed an exponentially increasing surface field and are consistent with this analysis approach.

4.1.6 Armature Rebound Conditions

With appropriate design, the increasing magnetic pressure due to flux compression will decelerate the expanding plasma armature until it is completely stopped and the motion is reversed. If this rebound process does not occur, the plasma will impact the reaction chamber wall, most probably with disastrous results. Clearly, stator impact is incompatible with repetitive operation and an estimate of the turnaround distance is essential.

At the turnaround point, we assume that the useful energy production per detonation has been transformed into magnetic energy. Thus,

$$W_{m,t} = W_{m,0} + hW_D \tag{81}$$

where $W_{m,t}$ is the magnetic field energy at the turnaround point

$$W_{m,t} = \left[\frac{1}{2} mH_t^2\right] V_t \tag{82}$$

and $W_{m,0}$ is the original magnetic field energy in the reaction chamber

$$W_{m,0} = \left[\frac{1}{2} mH_0^2\right] V_0 \tag{83}$$

W_D is the energy production per detonation, and η is the energy efficiency with which the available detonation energy is transformed into magnetic field energy. V_t and V_0 are the flux containment volumes at the turnaround point and at the beginning of armature expansion

$$V_t = p\left[\left(r_s + s_{f,s}\right)^2 - \left(r_t - s_{f,a}\right)^2\right] z \tag{84}$$

$$V_0 = p\left[r_s^2 - r_i^2\right] z \tag{85}$$

and z is the height of the reaction chamber. Furthermore,

$$W_D = w_D r_D p r_i^2 z \tag{86}$$

where w_D is the detonation energy per unit mass. Dividing Eq. (81) through by $W_{m,0}$ and evaluating Eq. (47) at the turnaround point yields the following relationship:

$$\frac{H_t}{H_0} = \frac{\left(r_s^2 - r_i^2\right)}{\left(r_s + s_{f,s}\right)^2 - \left(r_t + s_{f,a}\right)^2} = 1 + \frac{hW_D}{W_{m,0}} \tag{87}$$

The turnaround radius r_t is defined as the radial location at which Eq. (87) is satisfied.

4.1.7 Representative Calculations

As part of the Phase I work, the previously described skin layer methodology was implemented into a computer code for the purpose of carrying out exploratory performance calculations for the radial mode P^3G configuration. In the near term, it is anticipated that the first demonstration device will utilize high explosive detonation charges in order to establish scientific feasibility since ICF technology is still several years away from fruition. Indeed, it is believed that practical devices based on high explosive detonations can be developed with existing enabling technologies. Thus, Phase I calculations of P^3G performance were carried out for high explosive detonation charges, only. Calculations based on fusion microexplosions have been deferred to Phase II.

The chief difficulty encountered with high explosive plasma jets, is the limited magnetic Reynolds numbers that can be achieved. The detonation velocity of high explosive plasma jets is typically on the order of 10^4 m/s, and this level of performance can only be achieved through special shaped charge designs. The simplest and most common approach used in the production of high speed plasma jets is the conical shaped charge explosive illustrated in Fig. 13. Here, the detonation wave is initiated at the flat end of the charge and it propagates to the conical cavity where implosion of the reaction products along the axis of symmetry generates a high speed plasma jet in the forward direction.

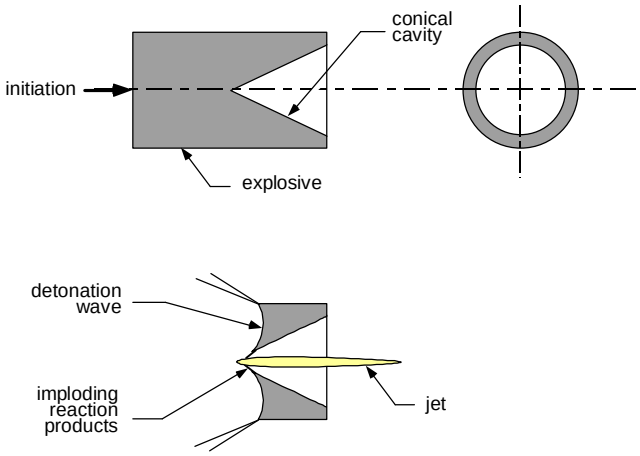

Figure 13: Illustration of a simple conical cavity shaped charge explosive.

Experimental investigations of shaped charge explosives as applied to MHD generator applications have been conducted in the past.[20] This included high speed imaging of the plasma jet and measurement of its velocity and electrical conductivity. The typical morphology of a plasma jet emanating from a cavity charge is illustrated in Fig. 14. In these tests, it has been observed that a cohesive, hot, rosy colored plasma slug is projected at speeds on the order of 3×10^4 m/s. This plasma slug is accompanied by a region of shock heated gas emitting a bluish glow due to the free electrons and a trail of luminous debris from the explosion follows closely behind. Figure 15 shows the measured electrical conductivity in a plasma jet from a 22° cavity charge of unseeded Composition-4. Note that the measured conductivity in the slug exceeded 10^4 mho/m. Inserting representative values for the jet velocity and electrical conductivity into the expression for the magnetic Reynolds number, as defined by Eq. (39), and assuming a reasonable length scale for a practical device, we find that

$$R_m = m_0 s_0 u_0 L_0 = 4p(10)^7 (10)^4 (10)^4 (10)^{-1} > 1 \tag{88}$$

Thus, it is plausible that a marginal level of magnetic Reynolds number can be achieved using simple unseeded shaped charges. This level could be boosted through the introduction of ionization seed as a conical liner to the shape charge and through pre-ionization of a gas, such as deuterium, in the reaction chamber. Furthermore, more advanced concepts for generating higher speed and more conductive plasma jets could be utilized.

Based on a critical evaluation of available high explosive technology for producing high velocity hot plasma jets, it has been concluded that the scientific feasibility of the proposed concept could be

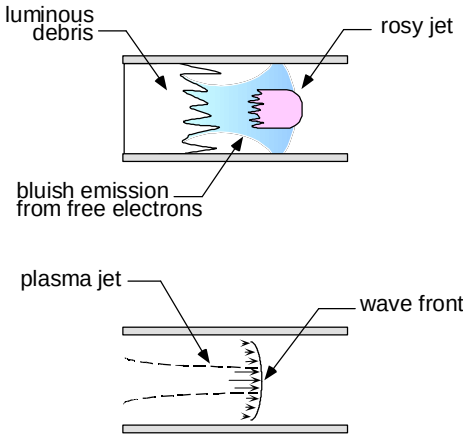

Figure 14: Typical morphology of a plasma jet emanating from a shaped charge explosive.

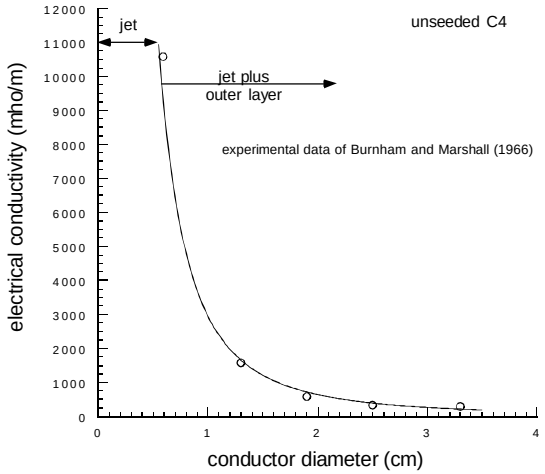

Figure 15: Measured electrical conductivity in a conical charge plasma jet of unseeded C4.[20]

established using a non-nuclear plasma source. It is also plausible that practical devices could be developed using non-nuclear detonations in order to generate the high levels of pulse power needed to initiate pulse fusion systems, such as ICF. A demonstration device along the lines of the Mark I configuration depicted in Fig. 16 would therefore seem a logical progressive step in this direction. This device is envisioned as a ½ m diameter reaction chamber, which uses colliding plasma jets from opposing high explosive charges to produce a radially expanding armature. The formation of a radially expanding plasma jet from two colliding jets has been previously demonstrated on a small scale. The observed collisional process in these experiments is illustrated in Fig. 17.

As a precursor analysis to the Mark I configuration, calculations based on the skin layer methodology were performed in Phase I. The calculations presumed an internal generator radius of 0.25 m and various stator materials were investigated. For the hypothetical HTSC stator material, a magnetic diffusivity value of 10^{-5} m^2/s was assumed. Typical parameters for high explosive detonations used in the calculations are summarized in Table V.

The variation in the flux coefficient as a function of the normalized armature radius is shown in Fig. 17. Calculations were performed for magnetic Reynolds numbers of 1 and 10 assuming stator materials of steel, copper, and a hypothetical HTSC. For a magnetic Reynolds number of unity,

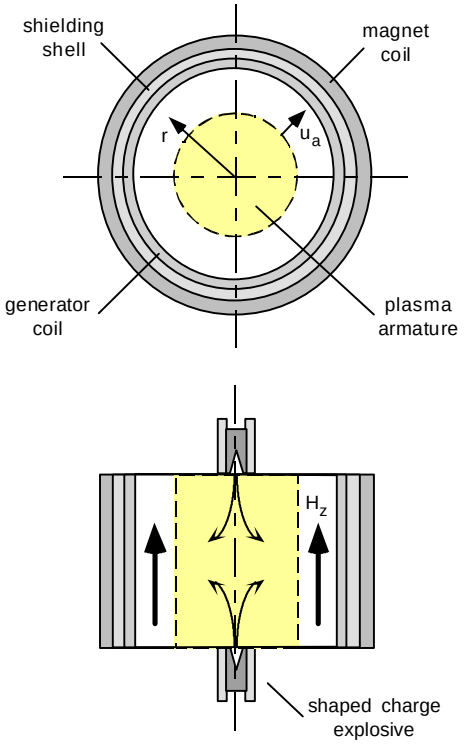

Figure 16: Mark I configuration for a radial mode explosively driven demonstration device.

Table V: High Explosive Characteristics

Density (ρ_D)	1700 kg/m^3
Specific Energy (w_D)	5×10^6 J/kg
Velocity (u_D)	1×10^4 m/s

we observe that the highly diffusive steel stator exhibits excessive flux diffusion losses. The copper stator, on the other hand, exhibits acceptable performance due to its much higher electrical conductivity. And the hypothetical HTSC stator ($D_m = 10^{-5}$ m^2/s) promises to boost flux compression efficiency beyond the level attainable with ordinary metals. When the magnetic Reynolds number is increased to 10, we see an increase in compression efficiency for all stator materials although the flux losses with the steel stator are still excessive. Apparently, significant flux compression can be accomplished at marginal magnetic Reynolds numbers when the stator material is sufficiently resistant to magnetic diffusion. Thus, it appears that a successful demonstration device could be developed, which utilizes a non-nuclear high explosive plasma jet source. If a suitable HTSC material can be found or developed that is resistant to magnetic field penetration when exposed to strong pulsed fields, the probability for achieving a successful demonstration are markedly improved. The preceding analysis is highly idealized, of course, and real hydrodynamic effects will lead to more pessimistic predictions with respect to the minimum required magnetic Reynolds number; however, the simplified analysis results are sufficiently encouraging to proceed with a Phase II program with a high degree of confidence. More detailed MHD calculations are deferred to Phase II.

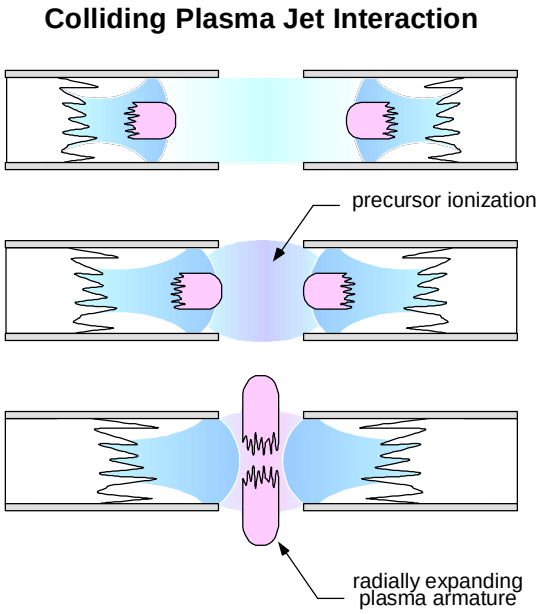

Figure 17: Illustration of plasma jet collisional process and radial armature formation.

Calculations for the armature turnaround radius as a function of initial seed field were carried out for both a copper stator and a hypothetical HTSC stator assuming an energy conversion efficiency of 50%. The results are presented in Fig. 19 for various magnetic Reynolds numbers. To avoid stator impact, we find that there is a minimum initial seed field the value of which depends on the magnitude of flux diffusion losses. With a good stator material and

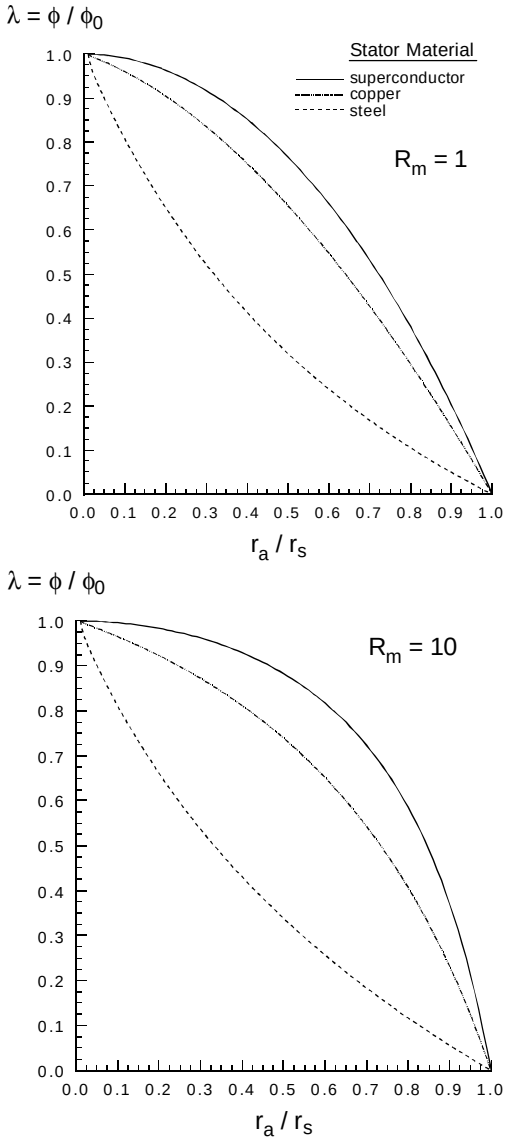

Figure 18: Computed flux coefficient for high explosive driven radial mode P3G.

high R_m, it is possible to reduce the seed field and minimize system size and weight.

5.0 Magnetic Diffusion in HTSC Materials

A key innovation of the P^3G concept is the use of a type-II HTSC stator material having a very low magnetic diffusivity. This approach has the potential to greatly reduce flux diffusion losses and markedly improve compression efficiency with a corresponding decrease in size, weight, and cost. Thus, simple Phase I laboratory experiments were designed to investigate the magnetic diffusivity characteristics of HTSC samples when exposed to strong pulsed magnetic fields. The basic configuration in these experiments, as illustrated in Fig. 20, is a hollow tube of test material surrounded by a solenoid, which can be used to create a pulsed external magnetic field on-demand. Measurement of the time varying magnetic field inside the tube, once the solenoid is pulsed, yields quantitative information with respect to the magnetic diffusivity properties of the material. In the following sub-sections, we describe an analytical treatment of the magnetic diffusion process through a conducting hollow cylinder and we provide a detailed description of the experimental arrangement.

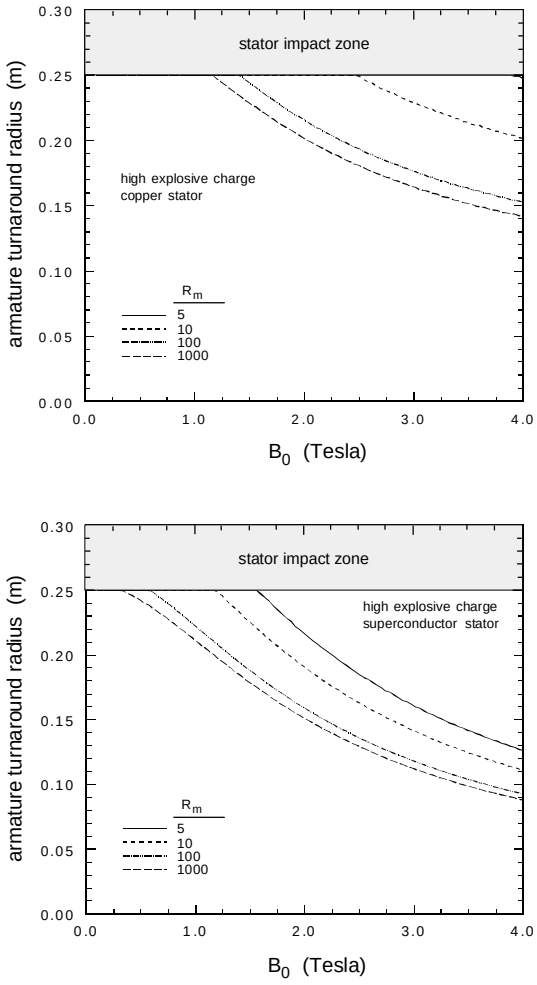

Figure 19: Computed armature rebound conditions for high explosive driven radial mode PPPG.

5.1 Analytical

To analyze the magnetic diffusion through a conducting hollow cylinder, we begin with Maxwell's electromagnetic relationships, as defined by Eqs. (21) - (24), and the isotropic medium relationships, as defined by Eqs. (25) – (26). By combining these relationships with Ohm's law and specializing to a cylindrical coordinate system, we obtain a magnetic diffusion equation in the same form as Eq. (38):

$$\frac{\partial^2 H}{\partial r^2}+\frac{1}{r}\frac{\partial H_z}{\partial r}=\frac{1}{D_m}\frac{\partial H_z}{\partial t} \qquad (89)$$

The initial/boundary conditions are as follows:

$$H_z(b,t)=H_0 \qquad (90)$$

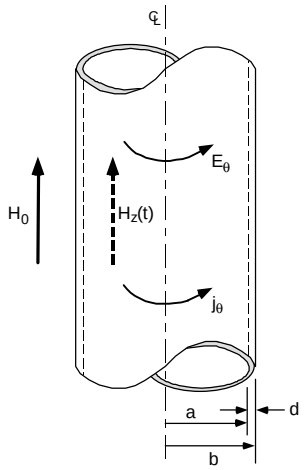

Figure 20: Illustration of experimental configuration for examining pulsed magnetic diffusion through a hollow conducting cylinder.

$$H_z(r,0) = 0 \tag{91}$$

The diffusion problem for a hollow cylindrical conductor with an outer radius b and an inner radius a requires an additional boundary condition at the inner surface. To obtain this condition, it is necessary to apply Faraday's Law of magnetic induction to the hollow interior of an infinitely long conductor where $\mu = \mu_0$ and H_z has the same value everywhere inside the cylinder.

First, integrate Eq. (22) over a surface s to obtain the form:

$$\int_s (\nabla \times \mathbf{E}) \cdot d\mathbf{s} = -\int_s \frac{\partial \mathbf{B}}{\partial t} \cdot d\mathbf{s} \tag{92}$$

but $\int_s (\nabla \times \mathbf{E}) \cdot d\mathbf{s} = \oint_c \mathbf{E} \cdot d\mathbf{l}$ according to Stoke's theorem. Thus,

$$\oint_c \mathbf{E} \cdot d\mathbf{l} = -\int_s \frac{\partial \mathbf{B}}{dt} \cdot d\mathbf{s} = -m_0 \int_s \frac{\partial \mathbf{H}}{\partial t} \cdot d\mathbf{s} \tag{93}$$

Let s be the surface defined by the intersection of a normal plane with the hollow interior such that

$$-m_0 A \frac{dH_z}{dt} = \oint_c \mathbf{E} \cdot d\mathbf{l} \tag{94}$$

where $A = \pi a^2$ is the cross-sectional area of the hollow interior. Using Eq. (21) and Ohm's Law in the interior region of the conductor we obtain

$$\nabla \times \mathbf{H} = s_0 \mathbf{E} \tag{95}$$

Since the tangential component of **E** must be continuous at the surface, Eq. (94) takes the form:

$$-m_0 p a^2 \left.\frac{dH_z}{dt}\right|_a = \frac{1}{s_0} \oint_c (\nabla \times \mathbf{H}) \cdot d\mathbf{l} \tag{96}$$

$$-(m_0 s_0) p a^2 \left.\frac{dH_z}{dt}\right|_a = \oint_c (\nabla \times \mathbf{H}) \cdot d\mathbf{l} \tag{97}$$

$$-\left(\frac{1}{D_m}\right) p a^2 \left.\frac{dH_z}{dt}\right|_a = -(2p\phi)\left[-\frac{\partial H_z}{\partial r}\right]_{r=a} \tag{98}$$

$$\left.\frac{dH_z}{dt}\right|_a = \frac{2D_m}{a}\left[\frac{\partial H_z}{\partial r}\right]_{r=a} \tag{99}$$

Equations (90), (91), and (99) represent the boundary and initial conditions for the diffusion of an axial magnetic field into a hollow conductor where the diffusion is governed by Eq. (89).

The solution to this system of equations is known from mathematical physics using the Laplace transform methodology. The field $H_z(t) = H_z(a,t)$, which is built up in the cavity of the conductor, can be given for $\mu_R = 1$ in the form:

$$H_z(a,t) = H_0 - 4H_0 \sum_{n=1}^{\infty} e^{-D_m a_n^2 t} \left\{ \frac{J_2(aa_n) J_0(ba_n)}{(aa_n)^2 \left[J_0^2(ba_n) - J_2^2(aa_n)\right]} \right\} \tag{100}$$

where the α_n are roots of

$$J_0(ba) Y_2(aa) - Y_0(ba) J_2(aa) = 0 \tag{101}$$

and J_n and Y_n are Bessel functions of the first and second kind of order n.

After a long enough time, such that

$$t \geq \frac{1}{D_m a_1^2} \tag{102}$$

it is sufficient to retain only the first (n = 1) term. The field growth in the conductor is then

$$H_z(a,t) \approx H_0\left(1 - e^{-t/t_1}\right) \tag{103}$$

where

$$t_1 = \frac{1}{D_m a_1^2} = \frac{b^2}{4pD_m} g \tag{104}$$

The parameter g, defined by

$$g = \frac{4p}{(ba_1)^2} \tag{105}$$

is a geometrical form factor which has been previously tabulated as a function of the ratio a/b.

Table VI: Tabulation of Geometric Form Factor as a Function of the Tube Radius Ratio.

a/b	g	a/b	g
0.00	2.173	0.65	1.587
0.05	2.173	0.70	1.431
0.10	2.172	0.75	1.253
0.15	2.170	0.80	1.052
0.20	2.164	0.85	0.8267
0.25	2.153	0.90	0.5766
0.30	2.133	0.95	0.3011
0.35	2.102	0.96	0.2430
0.40	2.059	0.97	0.1838
0.45	2.001	0.98	0.1236
0.50	1.926	0.99	0.0623
0.55	1.833	1.00	0.0000
0.60	1.720	–	–

For a type-II superconductor there exists a critical value of the applied field below which the field is unable to penetrate the superconductor. This value is designated as the shielding field, H*. Thus, the expression for the field growth rate in the conductor should be modified such that

$$H_z(a,t) = H_i^{\infty}\left(1 - e^{t/t_1}\right) \tag{106}$$

where

$$H_i^{\infty} = H_0 - H^* \tag{107}$$

is the asymptotic limit for the magnetic diffusion into a superconducting tube.

According to Bean's critical state model, the absolute value of the gradient of B equals the critical current density j_c and we can approximate the shielding field as

$$\frac{B^*}{(b-a)} \approx j_c \tag{108}$$

$$B^* \approx j_c(b-a) \tag{109}$$

Recall that the definition of the magnetic diffusivity is

$$D_m = \frac{1}{m_0 s} = \frac{r}{m_0} \tag{110}$$

where $\rho = \sigma^{-1}$ is the resistivity of the material and $\mu_0 = 4\pi\times10^{-7}$ H/m. The range of magnetic diffusivities encountered with typical type-II superconductors in the flux creep and flux flow mode are tabulated in Table VII.

The electrical resistivity in typical solid conductors can be expressed as the sum of a temperature independent component (ρ_d) and a temperature dependent component (ρ_T). The contribution of ρ_d is generally negligible at room temperature. A simple empirical conductivity law can be expressed in the form:

$$s \equiv \frac{1}{r} = \frac{s_0}{1+bQ} \tag{111}$$

where

$$Q = C_v T \tag{112}$$

Table VII: Magnetic Diffusivity Characteristics of Type-II HTSC

current flow regime	ρ ($\mu\Omega$·cm)	D_m (m^2/s)
flux creep ↑	10^{-4}	8×10^{-7}
	10^{-3}	8×10^{-6}
	10^{-2}	8×10^{-5}
flux flow ↓	10^{-1}	8×10^{-4}
	10^{0}	8×10^{-3}
	10^{1}	8×10^{-2}

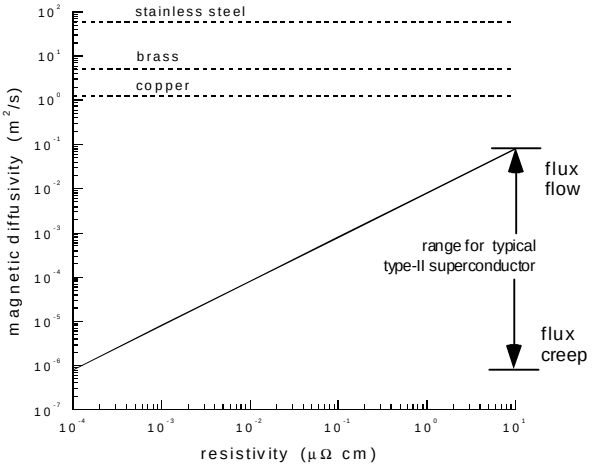

Figure 21: Comparison of magnetic diffusivities for common metals and the anticipated range for a HTSC material.

Here, σ_0 is the electrical conductivity at 0°C and β is an empirical parameter associated with a particular material. For most metals, the deviation of this simple linear relationship is generally smaller than ± 5%. Values of σ_0 and D_m for common metals were tabulated in Table II. Figure 21 compares the magnetic diffusivities of common metals and the range of values anticipated for a HTSC material.

In the small scale laboratory experiments, the tube size was as follows: length = 75 mm; wall thickness = 7.14375 mm; outside diameter = 30.1626 mm. This yields an inner radius of a = 0.079375 cm and an outer radius of b = 1.508125 cm. Thus, g = 1.8771 from Table VI and we may estimate the characteristic diffusion time according to Eq. (104). The characteristic diffusion times assuming a range of conductivity values for the HTSC material are summarized in Table VIII. The characteristic diffusion times for identically sized cylinders of common metals may be computed in a similar fashion, and these results are summarized in Table IX. Results for both the HTSC material and the metals are plotted in Fig. 22 for visual comparison. Actual diffusion characteristics of the HTSC material will depend on the behavior of the superconductor under strong pulsed fields. Based on the experimental efforts of previous researchers, D_m is anticipated to fall in the range of 10^{-5} to 10^{-3} m^2/s.

Table VIII: Anticipated Range of Characteristic Diffusion Times for HTSC Material

D_m (m^2/sec)	τ_1 (s)
$8(10)^{-7}$	$4.25(10)^{1}$
$8(10)^{-6}$	4.25
$8(10)^{-5}$	$4.25(10)^{-1}$
$8(10)^{-4}$	$4.25(10)^{-2}$
$8(10)^{-3}$	$4.25(10)^{-3}$
$8(10)^{-2}$	$4.25(10)^{-4}$

Table IX: Characteristic Diffusion Times for Common Metals

	D_m (m^2/sec)	τ_1 (s)
Copper	1.26	$2.70(10)^{-5}$
Aluminum	2.04	$1.67(10)^{-5}$
Brass	5.1	$6.66(10)^{-6}$
Stainless Steel	58	$5.68(10)^{-7}$

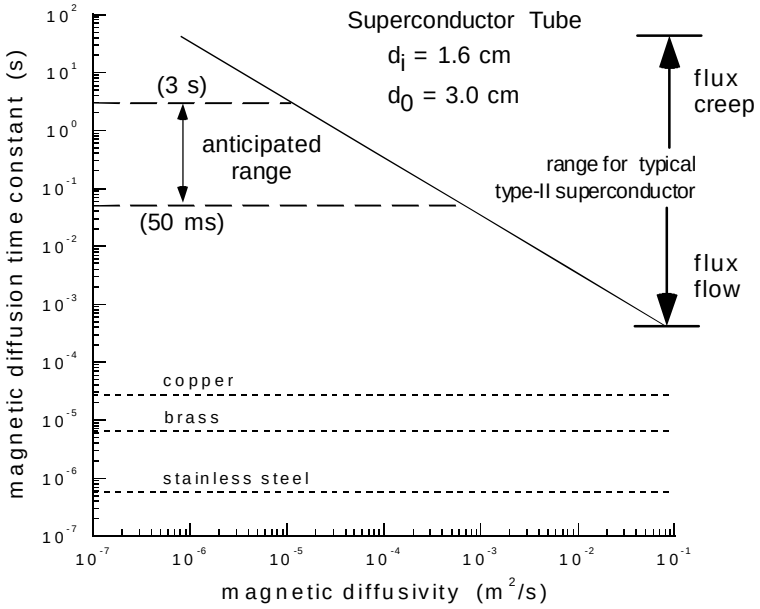

Figure 22: Characteristic magnetic diffusion time constant for magnetic field penetration through conducting hollow cylinders of various materials with g = 1.8771.

5.2 Experimental Approach

The objective of the experiments done for the Phase I study was to demonstrate that the diffusion characteristics of a high temperature type-II superconductor are acceptable for magnetic flux compression applications. In order to do this, we attempted to measure the magnetic diffusion rate through hollow YBCO (Yttrium-Barium-Copper-Oxide) and BSCCO ($Bi_2Sr_2CaCu_2O_x$) superconducting cylinders.

5.2.1 Replication of Cha and Askew Experiment

The experiments done by Cha and Askew [12] in their study of the transient response of a cylindrical BSCCO superconductor tube under a pulsed magnetic field were replicated for the Phase I study. We chose to study YBCO superconductors (in addition to BSCCO) because of the superior current density and critical properties of YBCO. Cha and Askew measured the induced current inside their BSCCO superconductor tube with a Rogowski coil and the magnetic field inside the tube with a Hall probe. Cha and Askew found that there is a time delay between the peak excitation current at field penetration and the magnetic field value inside the tube. Since the diffusion time of the magnetic field through the superconductor can be determined from the experimentally observed time delay, we sought to find the magnetic diffusion time constant of both YBCO and BSCCO superconductors. Replication of Cha and Askew's experimental data validates our test setup and procedures and serves as a basis for comparison of our results. To this end, the same experimental setup used by Cha and Askew was used for our experiments.

5.2.2 Apparatus and Experimental Procedure

The central part of the apparatus consists of a cylindrical superconductor (YBCO or BSCCO) and copper coil of 1150 turns surrounding the superconductor. A Hall probe is placed parallel to the centerline of the tube to measure the magnetic field inside the superconductor. A Gauss meter, which collects the magnetic field data from the Hall probe, was compared and calibrated to known magnets. A Rogowski coil is looped around the superconductor and coil to measure the induced current inside the tube. The variable resistor inside a 12 VDC power supply was adjusted so that 15 VDC was attained to power the Rogowski coil. The entire test section is submerged in liquid nitrogen at a temperature of 77 K in an insulated container. The liquid nitrogen reduces the coil's resistance to 1 Ohm. During testing, the top of the insulated container is covered to prevent heat transfer. Figure 23 shows a schematic of the test section. The copper coil is connected to a pulsed current source powered by 5 Volts with a 1 Ohm resistor. The switch for the pulsed current is turned on and current rushes through the solenoid coil. A current sensor is used to measure the applied excitation current. Photographs of the actual test section are presented in Figure 24.

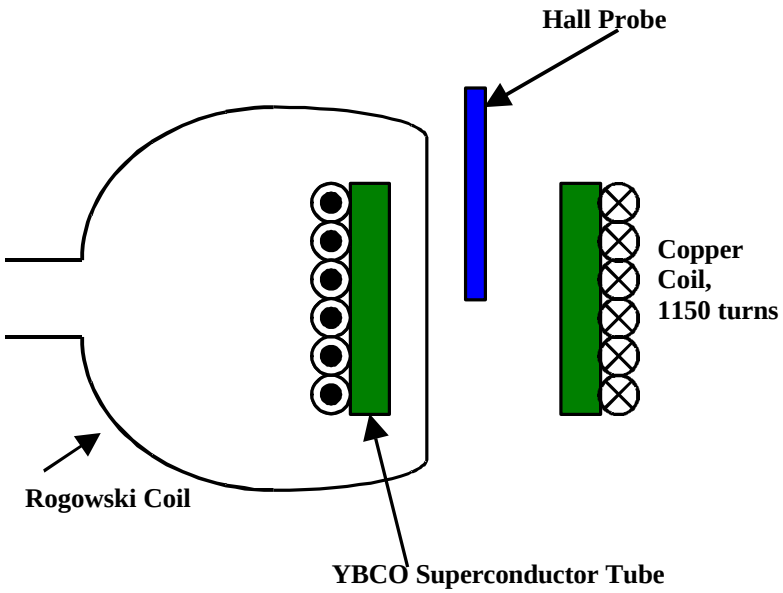

Figure 23 Schematic Diagram of Test Section

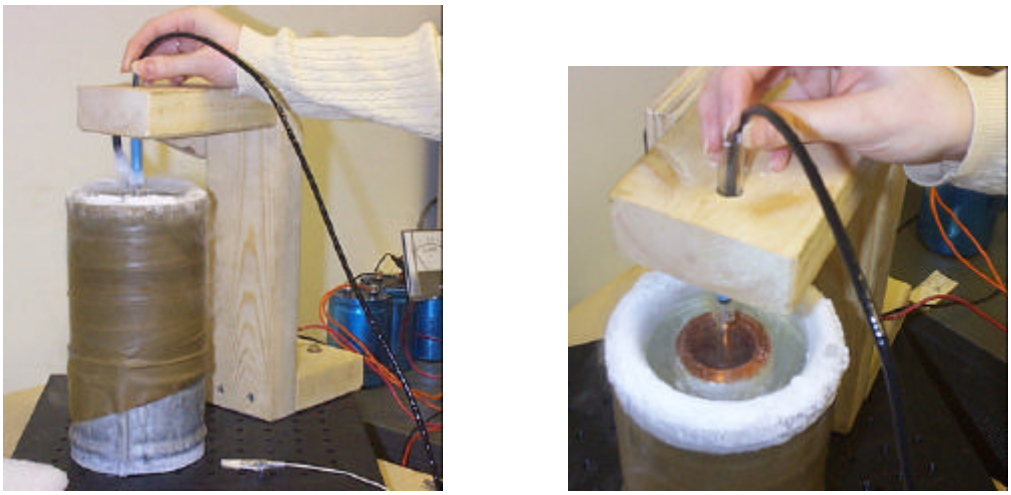

Figure 24: Actual Test Section

The experimental program consisted of two parts: (1) preliminary tests to check out the apparatus, procedures and data acquisition system and (2) actual tests done to measure the time delay between the peak values of excitation current and magnetic field inside the tubes. In order to check out the apparatus, tests were performed with metal tubes (aluminum, stainless steel, and copper) of the same geometry as the

superconductors. The tests consisted of placing the non-superconducting metal tubes inside the copper coil, pulsing the coil and measuring the magnetic diffusion rate through the tubes (Figure 25).

Figure 25: Tubes of Various Materials used in Preliminary Testing
From left to right: YBCO superconductor, stainless steel, aluminum, and copper

The different materials were tested in order to compare their magnetic diffusion rates to that of the superconductor. When measuring the excitation current and the magnetic field inside the superconductor, it is expected that there is a time delay between the two peaks; i.e. the peak magnetic field should occur after the current reaches its highest value. From the experimentally measured magnetic field value and time delay, the magnetic diffusion time constant through the tube can then be determined. The superconductor should have a greater resistance to the pulsed magnetic field and hence a longer diffusion time constant than the non-superconducting metal tubes.

The sample tubes were placed inside the solenoid coil and the circuit was pulsed, creating a magnetic field normal to the inside wall of the coil. This magnetic field diffused through each of the four sample tubes. The theoretical magnetic field, **B**, in a solenoid for a constant current, **I**, with N turns per length is given by:

$$\boldsymbol{B} = m_0 N \boldsymbol{I} \tag{113}$$

where μ_0 is the permeability of free space (= 4π x 10^{-7} N/A^2), N is 1150 turns over 7.62 cm, and **I** is 5 Amps. From this equation, the theoretical magnetic field inside the solenoid should be 948 Gauss (0.0948 Tesla). The pulsing of the circuit, and the resulting uncertainty of the applied current, should account for the difference in the theoretical and experimental magnetic fields.

Throughout the preliminary testing, there was difficulty measuring the magnetic diffusion rate through the YBCO superconductor specifically. The magnetic field seemed to diffuse through the superconductor with little or no resistance from the superconductor. At first it was assumed that this quick diffusion occurred because the YBCO superconductors made on-site were so porous. Since that time, new superconductors were made out of very fine YBCO powder. These superconductors had the desired densities of at least 5.7 g/cm^3, but they still did not seem to provide any resistance to the magnetic field as it passed through.

Next, it was thought that the data acquisition system was not sensitive enough to pick up the millisecond changes in the experimental apparatus. The data acquisition system was taken apart and each individual component was meticulously tested with an oscilloscope to see if the response times were satisfactory. After much testing and manipulation, it was determined that the response times were sufficient.

This left only one alternative – the superconductor was not providing enough shielding to prevent (virtually) immediate diffusion of the magnetic field. We concluded that we were not able to produce YBCO superconductors capable of resisting the magnetic field. Authors of similar papers on magnetic diffusion through superconductors were consulted about this problem, and they recommended Aventis, Inc. of Germany as a high quality producer of high temperature type-II superconductors. A BSCCO superconductor made by Aventis was subsequently purchased and is used to demonstrate the magnetic diffusion characteristics.

Tests done on the BSCCO superconductor indicate that there is a delay time of approximately 35 milliseconds between the excitation current and magnetic field inside the superconductor. Figure 26 shows the results of the tests. The aluminum tube shows a delay time of about 4 milliseconds. Thus, we may conclude that the BSCCO superconductor provides much greater resistance to magnetic field penetration than metals.

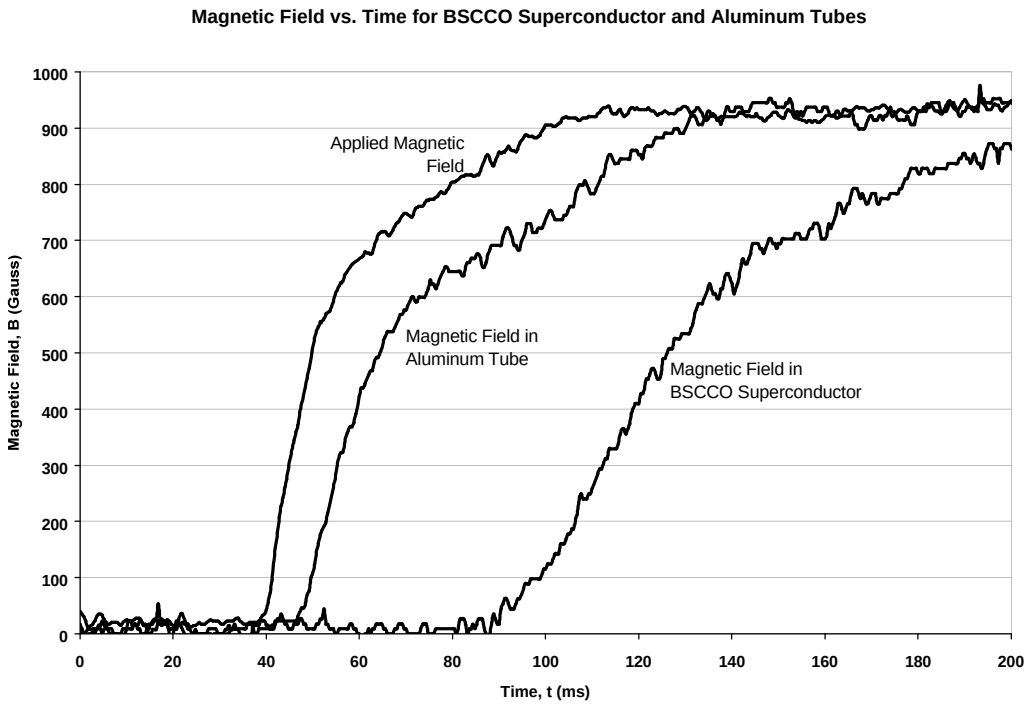

Figure 26: Comparison of Magnetic Diffusion Rates for a BSCCO and Aluminum Tube

6.0 Conclusions and Recommendations

The P^3G concept has the potential for significant payoffs in both the power and propulsion arenas. First, the analyses accomplished in this study indicate that 5 to 10 gigawatts of power can be generated with fuel consumption on the order of 1 gram per second with reasonable assumptions as to pulsing rate, coupling efficiency and burnup fraction. A similar analysis of the propulsion potential illustrated the capacity to reach specific impulses on the order of 10^6 seconds with appropriate thrust levels using comparable assumptions.

The analyses also served to identify the key technical issues associated with making this concept a reality. The use of plasma armatures does introduce substantial technical risks that must be addressed and overcome through research and development. The major uncertainties with the plasma armature approach are summarized below:

- achieving sufficiently high electrical conductivity in the detonation plasma
- magnetic field generation and control
- assurance of armature rebound
- suppression of Rayleigh-Taylor instabilities

The HTSC stators have associated with them, major uncertainties that may be categorized as follows:

- breakdown of HTSC under strong applied pulse fields
- hysteresis cycling of magnetization
- joule/neutron heating of the material
- structural integrity under cyclic loading
- bulk-processed vs. wire fabrication

Some experimentation was accomplished to address the feasibility of the HTSC stator. This experimentation yielded positive results for the BSCCO material but inconclusive for YBCO material. Testing with the BSCCO yielded anticipated magnetic penetration times through the tube. However, initial testing with YBCO (Yttrium-Barium-Copper Oxide) made at NASA MSFC failed to produce the desired magnetic diffusivity due to fabrication difficulties. Further research is needed to resolve whether the issues are the density or other manufacturing characteristics of the HTSC or the choice of the HTSC material.

Additional research is necessary to address these issues and fully assess the potential of this concept.

7.0 Acknowledgements

The authors gratefully acknowledge the support of NIAC and the contributions of Dr. Ron Litchford, an independent consultant to the Phase I project and Mr. Tony Robertson, HTSC material formulator and experimentalist for their advice and counsel on this program. We also acknowledge the cooperation and contributions of Aventis, Inc. manufacturer of the BSCCO superconducter tube used in our experiments.

8.0 References

[1]. F. Winterberg, "Rocket Propulsion by Thermonuclear Microbombs Ignited with Intense Relativistic Electron Beams," *Raumfahrtforschung*, Vol. 15, pp. 208-217, 1971.

[2]. R. A. Hyde, L. L. Wood, Jr., J. H. Nuckolls, "Prospects for Rocket Propulsion with Laser-Induced Fusion Microexplosions," AIAA Paper 72-1063, 1972.

[3]. A. R. Martin and A. Bond, "Nuclear Pulse Propulsion: A Historical Review for an Advanced Propulsion Concept," *Journal of the British Interplanetary Society*, Vol. 32, 1979, pp. 283-310.

[4]. A. R. Martin and A. Bond, "Project Daedalus: The Propulsion System; Part I: Theoretical considerations and calculations," in *Project Daedalus - Final Report on the the BIS Starship Study*, editor: A. R. Martin, Journal of the British Interplanetary Society, London, 1978, pp. S44-S61.

[5]. A. Bond and A. R. Martin, "Project Daedalus: The Propulsion System; Part II: Engineering design considerations and calculations," in *Project Daedalus - Final Report on the the BIS Starship Study*, editor: A. R. Martin, Journal of the British Interplanetary Society, London, 1978, pp. S63-S82.

[6]. R. A. Hyde, "A Laser Fusion Rocket for Interplanetary Propulsion," International Astronautical Fedration Paper IAF-83-396, 1983.

[7]. C. Orth, G. Klein, J. Sercel, N. Hoffman, K. Murray, and F. Chiang-Diaz, "Transport Vehicle for Manned Mars Missions Powered by Inertial Confinement Fusion," AIAA Paper 87-1904, 1987.

[8]. J. D. Lindl, *Inertial Confinement Fusion*, Springer-Verlag, New York, 1998.

[9]. I. R. Lindermuth and R. C. Kirkpatrick, "The Promise of Magnetized Fuel: High Gain in Inertia Confinement Fusion," *Fusion Technology*, Vol. 20, 1991, pp. 829-833.

[10]. R. A. Lewis, G. A. Smith, B. Dundore, J. Fulmer, and S. Chakrabarti, "Anitiproton-Catalyzed Microfission/Fusion Propulsion Systems for Exploration of the Outer Solar System and Beyond," AIAA Paper 97-3073, 1997.

[11]. Yu. P. Zakharov, A. G. Ponomarenko, H. Nakashima, Y. Nagamine, S. A. Nikitin, J. Wolowski, E. Woryna, "Direct Energy Conversion of Inertial Confinement Fusion and Experiments with Laser-Produced Plasma in Magnetic Fields," *Proceedings of the Ninth International Conference on Emerging Nuclear Energy Systems*, Herzliya, Israel, June 28 – July 2, 1998, pp. 384-389.

[12]. Y. S. Cha and T. R. Askew, "Transient Response of a High-Temperature Superconductor Tube to Pulsed Magnetic Fields," Physica C, Vol. 302, 1998, pp. 57-66.

[13]. H. Castro, L. Rinderer, E. Holguin, and J.-F. Loude, "Dynamics of Fast Flux Penetration in High-T_c Superconductors," Physica C, Vol. 281, 1997, pp. 293-302.

[14]. C. J. Everett and S. M. Ulam, "On a Method of Propulsion of Projectiles by Means of External Nuclear Explosions," LASL Report LAMS-1955, August 1955.

[15]. J. C. Nance, "Nuclear Pulse Propulsion," *IEEE Trans. On Nuclear Sci.*, NS-12, No. 1, 1965, pp.177-182.

[16]. S. L. Thompson and H. S. Lauson, "Improvements in the Chart D Radiation-Hydrodynamics Code II: A Revised Program," Sandia Laboratories Research Report SC-RR-71-0713, Feb. 1972.

[17]. S. I. Braginsky and V. D. Shafranov, "Plasma Motion in a Longitudinal Field," in *Plasma Physics and the Problems of Controlled Thermonuclear Reactions*, ed. By M. A. Leontovich, tr. From the Russian by A. J. Meadows, et. al. Permagon Press, London, 1959. Vol. II, pp. 39-125.

[18]. L. A. Artsimovich, "The Magnetic Flux in a Contracting Cylinder," in *Plasma Physics and the Problems of Controlled Thermonuclear Reactions*, ed. By M. A. Leontovich, tr. From the Russian by A. J. Meadows, et. al. Permagon Press, London, 1959. Vol. II, pp. 135-152.

[19]. A. D. Sakharov, "Magnetoimplosive Generators," *Soviet Phys.-Uspekhi* (English translation), Vol. 9, 1966, pp. 294-299.

[20]. M. W. Burnham and S. J. Marshall, "Some Experiments Related to Explosive Driven MHD Converters," *1st Conference on Megagauss Magnetic Field Generation by Explosives and Related Experiments*, Frascati, Italy, edited by H. Knoepfel and F. Herlach, Euratom publication EUR 2750.e, 1966, pp. 367-386.